ChemPubSoc Europe

DOI: 10.1002/cbic.201800593

CHEMBIOCHEM Full Papers

Identification of Small-Molecule Modulators of Diguanylate Cyclase by FRET-Based High-Throughput Screening

Matthias Christen,*[a] Cassandra Kamischke,[b] Hemantha D. Kulasekara,[b] Kathleen C. Olivas,[c] Bridget R. Kulasekara,[d] Beat Christen,[e] Toni Kline,[f] and Samuel I. Miller[b]

The bacterial second messenger cyclic diguanosine monophosphate (c-di-GMP) is a key regulator of cellular motility, the cell cycle, and biofilm formation with its resultant antibiotic tolerance, which can make chronic infections difficult to treat. Therefore, diguanylate cyclases, which regulate the spatiotemporal production of c-di-GMP, might be attractive drug targets for control of biofilm formation that is part of chronic infections. We present a FRET-based biochemical high-throughput screening approach coupled with detailed structure–activity studies to identify synthetic small-molecule modulators of the diguanylate cyclase DgcA from *Caulobacter crescentus*. We identified a set of seven small molecules that regulate DgcA enzymatic activity in the low-micromolar range. Subsequent structure–activity studies on selected scaffolds revealed a remarkable diversity of modulatory behavior, including slight chemical substitutions that reverse the effects from allosteric enzyme inhibition to activation. The compounds identified represent new chemotypes and are potentially developable into chemical genetic tools for the dissection of c-di-GMP signaling networks and alteration of c-di-GMP-associated phenotypes. In sum, our studies underline the importance of detailed mechanism-of-action studies for inhibitors of c-di-GMP signaling and demonstrate the complex interplay between synthetic small molecules and the regulatory mechanisms that control the activity of diguanylate cyclases.

Introduction

The second messenger cyclic dimeric guanosine monophosphate (c-di-GMP) mediates diverse bacterial cellular processes including antibiotic resistance, biofilm formation, extracellular carbohydrate and adhesin production, pilus- and flagellum-based motility, and cell cycle progression.[1–5] Signal integration into c-di-GMP networks is, in part, controlled by diguanylate cyclases (DGCs) that convert two molecules of GTP into c-di-GMP. The enzymatic activity of DGCs resides within a conserved domain consisting of the amino acid sequence glycine-glycine-aspartate-glutamate-phenylalanine (GGDEF) that forms the enzymatic active site. The GGDEF domain shares similarity to the PALM 4 domain found in other classes of nucleotide cyclases.[6–10] The apparent role of c-di-GMP in the cell cycle and the existence of many paralogous DGC enzymes controlling diverse cellular functions indicate that there is likely tight spatial and temporal regulation of c-di-GMP.[10–12] Bacterial genomes encode multiple GGDEF domains in proteins with signal-sensing domains.[13] However, the presence of multiple paralogues makes it difficult to study the signaling processing properties of c-di-GMP signaling networks by conventional genetic techniques. Therefore, chemical genetic approaches, inactivating each segment of the c-di-GMP signaling network, might be an attractive approach to studying the overall biological function of c-di-GMP. In pathogenic bacteria, cellular production of c-di-GMP is essential to maintain biofilm formation, especially under stressed conditions such as induction by aminoglycoside antibiotics.[1] Small molecules that effectively inhibit DGC activity have the potential to prevent biofilm formation, thus making DGCs interesting targets for the development of new classes of antimicrobial agents.

We developed a sensitive and robust FRET-based DGC activity assay and performed high-throughput (HT) screening on a comprehensive compound library to evaluate 27502 small molecules for inhibition of the *Caulobacter crescentus* DGC DgcA (CC3285). DgcA has been extensively characterized and therefore serves as a model enzyme for study of c-di-GMP-

[a] *Dr. M. Christen*
Eidgenössische Technische Hochschule Zürich, Department of Biology
Auguste-Piccard-Hof 1, 8093 Zürich (Switzerland)
E-mail: matthias.christen@imsb.biol.ethz.ch

[b] *C. Kamischke, Dr. H. D. Kulasekara, Prof. Dr. S. I. Miller*
University of Washington, Department of Microbiology
1959 NE Pacific St., Box 357710, Seattle, WA 98195 (USA)

[c] *Dr. K. C. Olivas*
Seattle Genetics, Inc.
21823 30th Drive SE, Bothell, WA 98021 (USA)

[d] *Dr. B. R. Kulasekara*
University of Washington, Department of Genome Sciences
1959 NE Pacific St., Box 357710, Seattle, WA 98195 (USA)

[e] *Prof. Dr. B. Christen*
Eidgenössische Technische Hochschule Zürich, Department of Biology
Otto-Stern-Weg-3, 8093 Zürich (Switzerland)

[f] *Dr. T. Kline*
Sutro Biopharma
310 Utah Avenue, Suite 150, San Francisco, CA 94080 (USA)

Supporting information and the ORCID identification numbers for the authors of this article can be found under https://doi.org/10.1002/cbic.201800593.

related phenotypic effects.[9,11,12,14] Similarly to the majority of DGC enzymes, DgcA is subject to high-affinity binding of c-di-GMP to an allosteric site (I site), which efficiently blocks enzymatic activity in a noncompetitive manner and is located distant from the catalytic pocket (A site). Mutational analysis of DgcA has provided convincing evidence that c-di-GMP binding to several conserved charged amino acids at the I site is a key mechanism for allosteric regulation of DGCs.[9]

Results

Development of a FRET-based biochemical high-throughput screen for monitoring c-di-GMP production

To identify small-molecule inhibitors of DgcA, we established a sensitive FRET-based activity assay. We have previously reported a FRET-based c-di-GMP biosensor, which we refer to here as the biosensor.[10] This biosensor consists of the c-di-GMP binding domain of the PilZ protein YcgR, C- and N-terminally tagged with mCYPet and mYPet fluorescent proteins. Binding of c-di-GMP to the YcgR domain induces a conformational change that alters the relative orientation of the external fluorescent subunit protein reporters, leading to a decrease in FRET efficiency. Thus, the fluorescence properties (535/470 nm emission ratio) of the biosensor reflect c-di-GMP levels. The biosensor exhibits a change in net FRET (nFRET) of −60.6%, with a binding constant of 198 nM for c-di-GMP and no detectable response to cyclic adenosine 3,5-monophosphate, cyclic GMP, or guanosine 5-triphosphate.[10]

To measure the suitability and performance of the biosensor for HT-capable DGC assay, we recorded kinetics of fluorescence emission ratio change in 384-well plates in a 20 μL reaction volume with 20 nM DgcA enzyme and 50 nM biosensor and followed the change in fluorescence at intervals of 1 min (Figure 1 A). Addition of 50 nM DgcA in the absence of GTP does not alter FRET efficiency (Figure 1 A, ○) whereas injection of 20 μM GTP induces a rapid change in FRET efficiency (Figure 1 A, ●). From the FRET ratio for the free and the c-di-GMP-saturated biosensor, we determined the corresponding increase in c-di-GMP (Figure 1 B). Our sensitive and robust FRET assay detects c-di-GMP production in the nM range and permits determination of initial rate kinetics at levels below the occurrence of allosteric c-di-GMP inhibition.

FRET-based HT screening and discovery of primary hits for diguanylate cyclase inhibition

A major challenge of biochemical HT screening is to achieve significance on large-scale experimental datasets for quality control and hit selection. Through prior screening, we determined plate uniformity, signal variability, and repeatability assessment assays for coefficient of variation (CV) and *Z* factor calculation. The average *Z* factor for three plates read on two consecutive days was 0.71, and the CV readings for high, medium, and low signal were well below 5%. The chemical library screened encompasses 27505 commercially available compounds derived from small-molecule chemical libraries

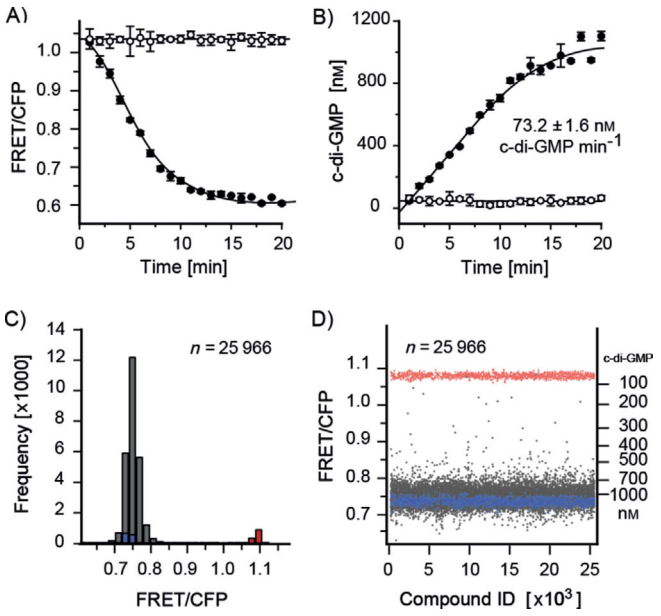

Figure 1. FRET assay for c-di-GMP. A) Kinetics of fluorescence emission ratio change (527/480 nm) measured in a 384-well plate format. Affinity-purified YcgR FRET biosensor was added in the presence of 20 nM DgcA enzyme and 20 μM GTP substrate (closed circles) or in the absence of GTP (open circles). B) Corresponding increase in c-di-GMP concentration derived from the change in fluorescence emission ration (535/470 nm). Above 800 nM c-di-GMP, allosteric product inhibition decreases the DGC activity of DgcA. Each graph shows the average of three independent measurements. The reaction volume per well was 20 μL in a 384-well Corning low-volume flat-bottomed plate. C) Histogram of the fluorescence emission ratio after 3 h incubation of 20 nM DgcA with 20 μM GTP in the presence of 50 μg mL^{-1} compounds (■) and 1% DMSO. Wells without added GTP substrate were used as positive controls (■); wells with exogenous c-di-GMP (5 μM) were used as negative controls (■). D) Plate uniformity of the HT screening. For every well, background fluorescence signal of the compound was measured prior to the addition of the FRET biosensor. Compounds with autofluorescence exceeding 7% of the FRET biosensor signal (535/470 nm) were discarded.

maintained at the Institute of Chemical Biology (ICCB) at Harvard University, Boston, MA, funded by the Regional Centers of Excellence in BioDefense and Emerging Infectious Disease (NSRB/NERCE). During screening, we first preincubated the DgcA enzyme with 200 nL compound (5 mg mL^{-1}) in DMSO and measured fluorescence emission ratio before and after addition of the biosensor to monitor fluorescence of chemical compounds and FRET at 470 and 535 nm. This second measurement will also detect compounds that mimic c-di-GMP agonists. After addition of 20 μM GTP, FRET was measured 3 h after incubation as an endpoint measurement (Figure 1 C, D; see also the Experimental Section). For a compound to be considered a hit, the following criteria had to be met: 1) compounds with c-di-GMP production below 300 nM after 3 h of incubation with DgcA and 20 μM GTP were considered strong hits, 2) duplicates were consistent with a difference in final c-di-GMP levels $<$100 nM, and 3) background fluorescence prior to addition of the FRET biosensor had not to exceed 7% of the FRET signal in CFP and YFP emission channels. We used total fluorescence as a quality control criterion to identify inherently fluorescent compounds. Of the 27502 compounds screened in duplicate, 1029 (3.7%) were removed from the analysis due to

autofluorescence. We identified 49 compounds (0.18%) as strong hits, with c-di-GMP levels below 300 nM after 3 h incubation with DgcA. An additional 241 compounds (0.87%) were classified as moderate inhibitors, with c-di-GMP levels below 400 nM after incubation with DgcA.

Selection of compound scaffolds for secondary assays and structure–activity relationship (SAR) studies

In selecting compounds for SAR studies, we placed a priority on compounds likely to be functioning through our target mechanism of action. We rejected cytotoxic or cytostatic compounds and favored those compounds that exhibited synthetic tractability and suitability for chemotype expansion. By these criteria, we selected 18 compounds out of 49 initial hits for confirmatory and secondary assays. We found that 38.9% (seven out of 18) had IC_{50} values smaller than 50 μM, whereas 22.2% (four out of 18) also had IC_{50} values smaller than 10 μM (Figure 2A). The results from our secondary assays led us to focus further structure–activity studies on the two scaffolds [2-oxo-2-(2-oxopyrrolidin-1-yl)ethyl] 1,3-benzothiazole-6-carboxylate (**1**) and 4-(2,5-dimethylphenoxy)-*N*-(4-morpholin-4-ylphenyl)butanamide (**2**), with IC_{50} values of 4.0 and 6.4 μM, respectively (Figure 2B and C). The concentration–response curve of compound **1** revealed complete inhibition of DgcA activity (Figure 2B). In contrast, compound **2** acts as a partial inhibitor

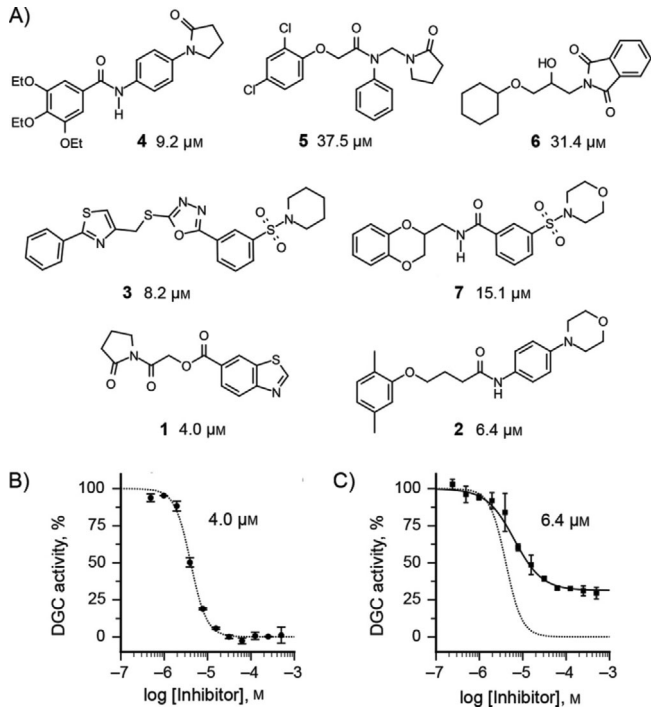

Figure 2. Inhibitors of the DGC enzyme DgcA. A) Structures of the small-molecule inhibitors **1**–**7** with IC_{50} values below 50 μM identified in the FRET screening. Out of these, the four compounds **1**–**4** exhibit IC_{50} values <10 μM. Scaffolds **1** and **2** were selected for subsequent SAR studies. B) The concentration–response curve of compound **1** ($IC_{50}=4$ μM) reveals complete inhibition against DgcA. C) Compound **2** ($IC_{50}=6.4$ μM) acts as partial inhibitor for DgcA. The corresponding concentration–response curve of **1** is shown as a dashed line.

for DgcA (Figure 2C), with 31.5% of DGC activity remaining in the presence of an enzyme-saturating inhibitor concentration. This indicates that upon binding of **2** the DgcA enzyme is converted into a modified but still partially functional enzyme·substrate·inhibitor complex, thus raising the possibility that **2** binds to a site distinct from the substrate binding site. For subsequent structure–activity studies, we chemically synthesized a set of 24 derivatives of compound **1** and 16 compounds with structural similarities to scaffold **2** (Experimental Section).

Characterization of SAR of scaffold 1

Structure–activity studies can be used to probe steric constraints imposed in the binding site and to reveal the molecular relationship between biological activity and structural properties of a ligand. Scaffold **1** contains a 2-oxo-2-(2-oxopyrrolidin-1-yl)ethyl component linked to a 1,3-benzothiazole-6-carbonyloxy unit (Figure 2A). We individually probed the 2-oxopyrrolidin-1-yl ring, the linker region, and the nucleobase-like 1,3-benzothiazole-6-carbonyloxy moiety for steric demand and biological activities. We tested the binding affinities of analogues of **1** by replacing the 2-oxopyrrolidin-1-yl ring by substituents R^1 (Table 1) and keeping the 2-oxoethyl linker and the 1,3-benzothiazole-6-carbonyloxy motif constant. Our selection of derivatives emphasized the pyrrolidin-1-yl group (as in **1a**), the 2-methylpropanamido group (as in **1b**), the cyclohexanecarboxamido group (as in **1c**), the benzamido group (as in **1d**), the 4-methylanilino group (as in **1e**) and the 2-methoxyanilino group (as in **1f**) replacing the 2-oxopyrrolidin-1-yl ring. We selected these residues for their steric demand and to probe for hydrogen bonding, hydrophobic interactions, and π stacking contacts.

The inhibitory potencies of the six analogues featuring 2-oxopyrrolidin-1-yl ring replacement are shown in Table 1. Many of the derivatives retained, but did not exceed, a level of potency comparable with that of **1**. For example, the replacement of the 2-oxopyrrolidin-1-yl moiety with a pyrrolidin-1-yl system in **1a** had only marginal effect on binding affinity, with a slight increase in IC_{50} from 4 to 17.1 μM (Table 1). These results suggest that the presence of an H-bond acceptor in the 2-oxopyrrolidin-1-yl component in **1** is not a prerequisite for mediating binding affinity to DgcA. Substitution of the 2-oxopyrrolidin-1-yl component with a 2-methylpropanamido system in **1b** does not affect binding affinity (IC_{50} of 3.6 versus 4.0 μM). However, introduction of substituents with increased steric demand, such as the cyclohexanecarboxamido motif in **1c** or the benzamido group in **1d**, in each case shows a tenfold reduction in binding affinity, to 47.2 and 48.5 μM, respectively. To test whether the decrease in binding affinity is caused by steric hindrance at the binding site, we reduced the steric load and introduced the 4- and 2-methoxyanilino analogues **1e** and **1f**, respectively. As expected, we observed increases in affinity, to 8.5 and 10.7 μM, respectively.

Thus, it seems that the 2-oxopyrrolidin-1-yl ring of scaffold **1** can be replaced by alternative substituents without dramatically altering binding affinity. However, although several substitutions of the 2-oxopyrrolidin-1-yl ring did not affect binding

Table 1. Exploration of 2-oxopyrrolidin-1-yl ring substitutions in the **1** scaffold.

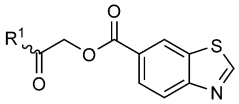

Cmpd	R^1	IC_{50} ± SD [μM][a]	Hill coeff.[b]	Activity ESI [%][c]
1		4.0 ± 0.2	2.34 ± 0.19	1.40 ± 0.1
1a		17.1 ± 1.2	2.57 ± 0.40	6.04 ± 0.46
1b	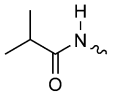	3.6 ± 0.6	1.65 ± 0.38	61.74 ± 4.31
1c	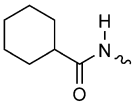	47.2 ± 8.4	1.46 ± 0.26	9.01 ± 0.78
1d	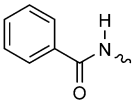	48.5 ± 3.8	2.89 ± 0.32	14.64 ± 0.74
1e	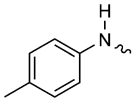	8.5 ± 0.7	2.93 ± 0.48	3.09 ± 0.25
1f	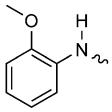	10.7 ± 2.5	1.48 ± 0.13	59.42 ± 1.61

[a] All experiments to determine IC_{50} values were run with at least duplicates at each compound dilution. IC_{50} values were averaged when determined in two or more independent experiments. [b] Hill coefficients obtained upon fitting the concentration–response curves. [c] DGC activities of the enzyme·substrate·inhibitor complexes.

affinity, they had dramatic effects on the residual activities of the enzyme·inhibitor·substrate complexes (Table 1). For example, replacement of the 2-oxopyrrolidin-1-yl moiety of **1** (IC_{50} of 4 μM) with the 2-methylpropanamido system in **1b** (IC_{50} of 3.6 μM) shifts the activity of the enzyme·inhibitor·substrate complex from 1.4% to 61.7% (Table 1). Similar effects were observed for the 4- and 2-methoxyanilino derivatives **1e** and **1f**, with IC_{50} values of 8.5 and 10.7 μM, respectively. Compound **1e** exhibits almost complete inhibition with only 3.1% DGC activity upon inhibitor saturation, whereas **1f** functions as a partial inhibitor for DgcA, with 59.4% activity remaining in the enzyme·substrate·inhibitor complex. These results suggest that **1f** binding converts the DgcA enzyme into a modified but still functional enzyme·substrate·inhibitor complex. Simultaneous binding of substrate and inhibitor indicates that **1** and its derivatives likely bind to a site distinct from the substrate binding site of DgcA.

Effects of benzothiazole substitutions in scaffold 1 on binding affinity and modulation of DgcA

Next, we replaced the 1,3-benzothiazole-6-carbonyloxy moiety on **1** and chemically synthesized 12 derivatives containing alternative heterocycle and phenyl substituents (Experimental Section). We introduced various heterocycles with both 5- and 6-substituted (benzothiazole numbering) carboxylato groups. In addition, we altered the positions and types of heteroatoms present in the heterocycles. For every derivative, we measured dose–response curves and maximum inhibition values with the FRET-based DGC assay. The inhibitory activity data and maximum inhibition values are summarized in Table 2. Whereas compound **1i**, in which the 1,3-benzothiazole-6-carbonyloxy component was substituted with a 2-methyl-1,3-benzothiazole-5-carbonyloxy motif, exhibited decreased inhibitory effects (IC_{50} = 52.7 μM), we observed almost identical IC_{50} values in the cases of the 1,3-benzoxazole-6-carbonyloxy derivative **1g** and the 2,3-dihydrobenzofuran 5-carbonyloxy derivative **1j**, with 3.1 and 4.4 μM, respectively (Table 2). However, **1g** and **1j** failed to block DGC activity effectively, and DgcA remained partial active in the presence of the inhibitors (87.7% and 92.2%, respectively). These findings suggest that **1g** and **1j** both act as silent allosteric modulators (SAMs) of DgcA (Table 2). Furthermore, we found that substitution with the 1*H*-indole-5-carbonyloxy group (as in **1k**), the 1-methyl-1*H*-indole-5-carbonyloxy group (as in **1l**), the 1-methyl-1*H*-benzimidazole-5-carbonyloxy group (as in **1m**), the isoquinoline-6-carbonyloxy group (as in **1n**), and the quinoxaline-6-carbonyloxy group (as in **1o**) resulted in strongly reduced binding affinities towards DgcA but maintained those analogues' function as negative modulators. Similarly, alteration of the carbonyloxy side chain to a 1,3-benzothiazole-5-carbonyloxy unit in the case of **1p** had a dramatic effect and decreased the binding affinity from 4 to 626 μM. These findings underline the isosteric importance of the 1,3-benzothiazole-6-carbonyloxy component in mediating the inhibitor potency of **1**.

We next introduced benzoyloxy, 4-(dimethylamino)benzoyloxy, and 4-nitrobenzoyloxy moieties in **1h**, **1q**, and **1r**, respectively (Table 2). Surprisingly, whereas the introduction of these substituents resulted in rather moderate binding affinities, we observed that DgcA activity increased in the presence of these compounds to activities higher than in their absence (118, 176, and 156%, respectively), thus suggesting that these compounds act as positive modulators of the DGC enzyme.

In the last group of derivatives, we investigated effects of linker modifications. The parent compound **1** contains an ester bond, which harbors the intrinsic risk of cleavage by cellular esterases. A nonhydrolyzable amide analogue should provide much better stability towards proteolysis by esterases. Therefore, we synthesized the nonhydrolyzable amide derivative **1s** (Table S1 in the Supporting Information) and tested its inhibitory properties against DgcA. We found that replacement of the ester bond with an amide increased the IC_{50} from 4 to 31.6 μM and resulted in a partial inhibitor with 48% residual activity of the enzyme·inhibitor·substrate complex. This suggests that differences in hydrogen-bond-forming properties or

Table 2. Substitution of the 1,3-benzothiazole component in scaffold **1** with alternative heterocycle and aryl substituents.

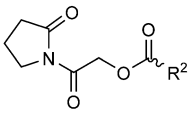

Cmpd	R^2	IC_{50} AC_{50} ± SD [μM][a]	Hill coeff.[b]	Activity ESI [%][c]
Negative allosteric modulators				
1i	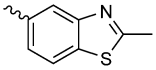	52.9 ± 10.7	2.72 ± 1.28	68.1 ± 8.8
1k	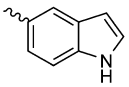	323.5 ± 39	2.37 ± 0.30	6.3 ± 0.4
1l	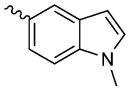	300.5 ± 37.7	1.65 ± 0.38	61.74 ± 4.31
1m	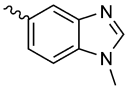	82.2 ± 14.6	1.52 ± 0.28	9.01 ± 0.78
1n	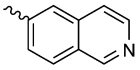	179.4 ± 10.5	2.06 ± 0.15	0.0 ± 2.0
1o	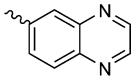	344.0 ± 19.9	2.22 ± 0.16	0.0 ± 0.7
1p	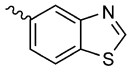	626.5 ± 49	1.48 ± 0.13	59.42 ± 1.61
Silent allosteric modulators				
1g	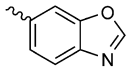	3.1 ± 0.7	2.35 ± 0.82	87.7 ± 4.2
1j	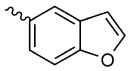	4.4 ± 2.2	2.05 ± 0.12	92.2 ± 0.6
Positive allosteric modulators				
1h		238.1 ± 72.0	2.02 ± 0.19	117.9 ± 1.4
1q	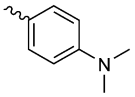	222.4 ± 85.6	2.51 ± 0.68	176.1 ± 3.3
1r	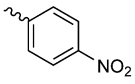	55.5 ± 13.6	2.01 ± 0.18	156.4 ± 1.7

[a] All experiments to determine IC_{50} and AC_{50} values were run at least in duplicate at each compound dilution. IC_{50} and AC_{50} values were averaged when determined in two or more independent experiments. [b] Hill coefficients obtained by fitting the concentration–response curves. [c] DGC activities of the enzyme·substrate·inhibitor complexes.

increased structural flexibility of the C–O–C bond might be important determinants for the affinity and potency of the scaffold **1**. Similarly, the introduction of a methyl group in the linker region, as in **1t**, or extension of the linker space between the 2-oxopyrrolidin-1-yl and the 1,3-benzothiazole-6-carbonyloxy components, as in **1u**, completely abolished the binding affinity, thus suggesting that both the composition of the linker region and the relative orientation and distance between the 2-oxopyrrolidin-1-yl and the benzothiazole moieties are critical determinants of binding affinity for DgcA.

Although the parent compound **1** exhibits characteristics of a complete inhibitor, we created a panel of derivatives of **1** with diverse effects on DgcA activity. Several analogues of the scaffold **1** exhibit partial inhibition, whereas some act as silent modulators or even function as positive modulators of DgcA. Thus, it seems likely that, rather than binding in a competitive mode, compounds of the scaffold **1** interact with an allosteric site of DgcA. The fact that these structurally very similar compounds exert diverse effects on the activity of the enzyme·inhibitor·substrate complexes suggests a model in which an allosteric binding site of DgcA is highly responsive to slight conformational changes. Substitution, for example, of a single sulfur atom in the benzothiazole moiety of **1** with oxygen in **1g** preserves binding affinity (IC_{50} values of 4 and 3.1 μM, respectively) but increases the activity of the enzyme·inhibitor complex more than 60-fold from 1.4 to 87.7%. Similar effects are observed with **1** and **1b**: substitution of the 2-oxopyrrolidin-1-yl system with 2-methylpropanamido group does not affect IC_{50} values but increases the activity of the enzyme·inhibitor complex from 1.4 to 62%.

In conclusion, our structure–activity studies on scaffold **1** suggest a model in which subtle substitutions within distal 2-oxopyrrolidin-1-yl and benzothiazole moieties both affect affinity and determine whether derivatives of the scaffold **1** act as negative, silent, or positive allosteric modulators of DgcA activity.

Structure–activity relationships of scaffold 2

Similarly to several of the derivatives of **1**, the second scaffold—4-(2,5-dimethylphenoxy)-*N*-[4-(morpholin-4-yl)phenyl]butanamide (**2**)—also acts as a partial inhibitor. Thus, we hypothesized that **2** might bind through a mechanism similar to that observed for **1** and its derivatives **1a**–**u**. If both scaffolds bind to the same regulatory site of DgcA, it should be feasible to alter their modulatory effect by exchanging the positions and modifications of the aryl substituents in **2** to generate derivatives with negative, silent, or even positive allosteric modulatory effects. We tested a set of 14 analogues of **2** by altering the aryl substituents on R^1 and R^2 and keeping the butanamide linker constant (Table 3).

The parent scaffold **2** harbors two methyl substituents as R^1 and one 4-morpholin-4-yl substituent as R^2 (Table 3). We found that removal of all aryl substituents, in **2c**, does not significantly alter the binding affinity (10.6 vs. 6.4 μM) or the activity of the enzyme-modulator-bound complex (38.6 vs. 31.4%). For compound **2d**, with a single 4-methyl substituent, we observed a binding affinity of 207 μM. For the 2-methyl-substituted derivative **2e**, we determined an IC_{50} of 2.2 μM. The steric load of a single methyl group at the *para* position barely accounts for a 100-fold difference in binding affinity between **2d** and **2e**. Similar results were observed for alterations in the methyl substitution pattern in compound **2a**. Movement of a methyl group from the 5- to the 4-position as R^1 preserved affinity at 11.7 μM but meanwhile increased the activity of the

Table 3. Exploration of aryl substituents in **2** and their modulatory effects on DGC activity.

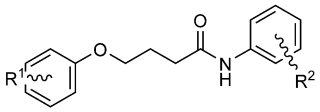

Cmpd	R^1	R^2	IC_{50}/AC_{50} ± SD [μM][a]	Hill coeff.[b]	Activity ESI [%][c]
Negative allosteric modulators					
2	2-CH_3, 5-CH_3	morpholin-4-yl	6.4 ± 0.5	1.36 ± 0.13	31.4 ± 1.3
2a	2-CH_3, 4-CH_3	morpholin-4-yl	11.7 ± 1.8	2.01 ± 0.08	69.8 ± 0.7
2c	H	H	10.6 ± 0.8	2.45 ± 0.34	38.6 ± 2.1
2d	4-CH_3	morpholin-4-yl	207.0 ± 77.8	2.42 ± 1.35	42.2 ± 9.3
2e	2-CH_3	morpholin-4-yl	2.2 ± 0.5	2.34 ± 1.04	63.3 ± 8.5
2f	2-CH_3, 5-CH_3	3-$COCH_3$	127.3 ± 0.9	1.29 ± 0.10	5.9 ± 0.4
2g	H	4-$NHCOCH_3$	620.3 ± 77.2	1.19 ± 0.10	8.3 ± 2.5
2h	4-OCH_3	4-$NHCO(C_3H_5)$	271.1 ± 13.9	0.96 ± 0.07	1.2 ± 0.0
2i	H	4-$N(CH_3)_2$	4.4 ± 2.2	2.05 ± 0.12	92.2 ± 0.6
Silent allosteric modulator					
2j	H	4-morpholine	12.1 ± 5.2	1.99 ± 0.04	95.5 ± 0.1
Positive allosteric modulators					
2k	H	2-morpholine	69.9 ± 5.8	2.87 ± 0.61	172.6 ± 2.4
2l	4-OCH_3	2-morpholine	46.8 ± 3.4	2.84 ± 0.46	167.3 ± 2.2
2m	H	3-sulfonyl-morpholine	25.0 ± 5.3	2.06 ± 0.15	142.0 ± 1.4
2n	4-*t*Bu	2-hydroxy, 5-sulfonyl-morpholine	25.4 ± 3.5	2.08 ± 0.51	146.5 ± 4.4
2b	H	2-OCH_3, 5-sulfonyl-morpholine	12.5 ± 1.0	1.62 ± 0.04	147.8 ± 3.7

[a] All experiments to determine IC_{50} and AC_{50} values were run at least in duplicate at each compound dilution. IC_{50} and AC_{50} values were averaged when determined in two or more independent experiments. [b] Hill coefficients obtained upon fitting the concentration–response curves. [c] DGC activities of the enzyme·substrate·inhibitor complexes.

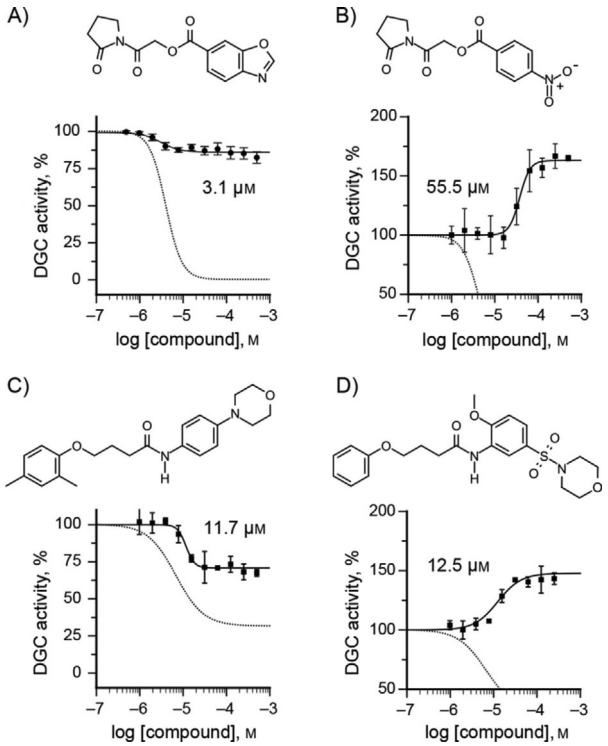

Figure 3. Examples of silent, negative, and positive allosteric modulators (SAMs, NAMs, and PAMs, respectively) of the DGC enzyme DgcA. A) Structure of and concentration–response curve for the 1,3-benzoxazole-6-carbonyloxy derivative **1g**, a silent allosteric regulator of DgcA. B) Representative example of an allosteric activator of the scaffold **1**. The 4-nitrobenzoic acid derivative of **1h** (**1r**) acts as a positive allosteric regulator with AC_{50} of 55.5 μM. The concentration–response curves for the parent 1,3-benzothiazole-6-carbonyloxy **1** are shown as dashed lines in (A) and (B). C) Structure of and concentration–response curve for **2a**. Alteration of the two methyl substituents from a 2,5 to a 2,4 arrangement in the **2** scaffold increases the residual activity of the enzyme·substrate·inhibitor complex from 31.4% in **2** (-----) to 69.8% in **2a** (●). D) The 2-methoxy-5-(morpholine-4-sulfonyloxy) derivative **2b** is a positive allosteric regulator with AC_{50} of 12.5 μM. Concentration–response curves for the parent **2** are shown as dashed lines in (C) and (D).

enzyme·inhibitor complex from 31.4 to 69.8%. However, removing either one of the methyl substituents in **2a** resulted in derivatives with differences in binding affinity.

We further expanded the spectrum of negative allosteric modulators by introducing 3-acetyl substitution, in **2f**, 4-acetamido substitution, in **2g**, 4-cyclopropanecarboxamido substitution, in **2h**, and 4-dimethylamino substitution, in **2i**, at R^2. With the exception of the dimethylamino derivative **2i**, which retained 71.1% DGC activity, all compounds had inhibitor-bound activities smaller than 8.5%. Substitutions patterns in the group of negative allosteric modulators of the scaffold **2** differ with respect to steric demand and hydrogen-bonding properties; however, most of them contain *para*-substituents at R^2. We investigated the modulatory effects of *ortho*- and *meta*-substitution at R^2 and introduced either morpholin-2-yl at the *ortho*-position, in **2k** and **2l**, or 3-sulfonyl-morpholinyl substitution at the *meta*-position, in **2m**. Upon measuring dose–response curves and maximum inhibition values by use of the FRET based DGC assay, we observed increasing DGC activity, between 142 and 172%, for all *meta*- and *ortho*-substituted derivatives **2b** and **2k**–**n**, thus suggesting that these compounds act as positive modulators of the DGC enzyme (Figure 3D and Table 3).

Mechanism of inhibition for 1 and 2

Our results suggest that both scaffolds **1** and **2** are able to bind to the DgcA enzyme at a site distinct from the GTP binding pocket. Although it might be possible for such mixed-type modulators to bind at the active site, allosteric modulation generally results from compounds binding to different sites. An attractive candidate for such an allosteric binding site is the product inhibition site (I site) of DgcA. Product inhibition by c-di-GMP is a general regulatory mechanism of many DGC enzymes and requires a RXXD motif that forms a turn at the end of a short five-amino-acid linker that directly connects the I site with the conserved catalytic A site residues GG(D/E)EF.[9] Previous molecular simulations on the DGC PleD in the presence and in the absence of c-di-GMP revealed a significant decrease in mobility for both I and A site residues upon complex formation.[9] This suggests that dynamic coupling between the two sites through the short connecting β-strand and a balance-like movement could be responsible for direct information transfer. To investigate whether allosteric binding of scaffolds **1** and **2**

affects substrate binding or maximum reaction rate of DgcA at the active site, we performed DGC inhibition assays in the presence of increasing concentrations of substrate GTP (Figure 4, Tables S2 and S3). For **1** we observed a decrease in affinity for substrate binding as well as a reduction in maximum rate of the DGC reaction (Figure 4A, B and Table S2). Thus, binding of **1** likely destabilizes the divalent Mg^{2+} carboxylate complex that is part of the transition state, as well as affecting the conformation of additional residues at the guanine binding pocket, leading to a reduction in binding affinity for the substrate GTP. In contrast, we found that binding of **2** affects only the K_m for GTP but does not impair maximum velocity of enzyme catalysis (Figure 4A, B and Table S3). This suggests that binding of **2** at the allosteric site likely induces conformational changes at the active site, resulting in reduced affinity for substrate binding, but probably maintains the three-dimensional conformation of catalytic residues during the transition state.

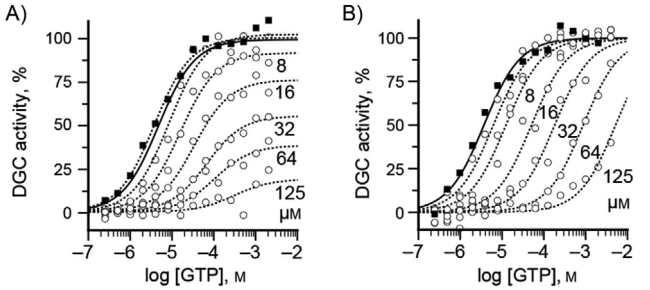

Figure 4. Effects of **1** and **2** on substrate binding and maximum reaction rate of DgcA. Corresponding plot of the initial velocity versus GTP concentration. A) The presence of **1** decreases affinity for substrate binding and maximum rate of DGC reaction (Table S3). B) In contrast to that of **1**, binding of **2** affects only the K_m for GTP but does not affect maximum velocity (Table S3).

Discussion

Thanks to their importance in governing amounts and spatiotemporal distribution of c-di-GMP, DGC enzymes are considered important targets for control of biofilm formation and antibiotic persistence phenotypes. Our results demonstrate that fluorescence-protein-based FRET biosensors can be employed as powerful analytical tools to detect c-di-GMP in the nanomolar range and to monitor performance of diguanylate cyclase enzyme reactions in a 384-well format in the low nanomolar range. With increasing numbers of available assays that monitor fluctuations in cellular c-di-GMP levels,[10,15–17] we can begin to identify effective approaches by which to discover potent small-molecule modulators of c-di-GMP signaling and to monitor their phenotypic effects and influence on cellular c-di-GMP signaling patterns. In addition to c-di-GMP, many other cyclic nucleotide second messengers, such as cAMP, cGMP, c-di-AMP, and cGAMP, currently lack high-throughput-screening (HTS)-capable analytical methods that allow in situ detection of their levels during enzymatic assays or in complex biological samples. In the future, similar FRET-based biosensors could provide interesting alternatives to current existing assays. Often, receptor proteins are known to recognize their cognate signaling molecule with high specificity. Insertions of these receptor domains between FRET pairs of fluorescent proteins should lead to new biosensor designs that detect their cognate signaling molecules with high specificity.

Several strategies for the chemical synthesis of c-di-GMP derivatives as potential inhibitors targeting DGC have been reported,[18,19] and a number of small-molecule inhibitors of DGC activity have been described previously.[20–24] Although these compounds were valuable research tools, their potencies and pharmaceutical properties were insufficient to determine the impact of DGC inhibition in vivo. Originally our HT screen was designed to discover inhibitors of diguanylate cyclases. However, our subsequent structure–activity studies unraveled a panel of 44 compounds that exert surprising variations in modulatory effects on DgcA activity. Among them is one complete negative allosteric modulator (**1**, with IC_{50} of 4 μM), two partial negative regulators (**1b** and **1c**, with 3.6 and 2.2 μM), two silent allosteric modulators (**1g** and **1j**, with IC_{50} values of 3.1 and 4.4 μM), and one positive allosteric modulator of DgcA activity (**2b**, with AC_{50} of 12.5 μM).

In terms of activities, we discovered remarkable diversity between compounds, with even small chemical substitutions on side chains reversing effects between inhibition and DGC activation. These results emphasize the importance of dynamic conformational changes rather than static three-dimensional structure for the biological function of DGC modulators. In scaffold **1**, for example, substitution of a single sulfur atom in benzothiazole with oxygen increases the activity of the modulator bound complex over 60-fold while maintaining binding affinity at 4 μM. In the **2** scaffold, shifting a single *para*-substituent to the *ortho*-position converted the silent modulator **2j** into the activator **2k**. Whereas the I site has previously been reported as an inhibitory site,[8,10] our analysis reveals that DGC enzymes are subjected to additional layers of allosteric regulation. We demonstrate that several synthetic small molecules are able to activate DgcA allosterically, rather than inhibiting. It is interesting to speculate that other endogenous molecules or protein domains might adopt a similar mechanism of action and function as endogenous allosteric activators of DGC enzymes coupling DGC activity to distinct cellular signaling inputs. In fact, several GGDEF-domain-containing proteins, despite harboring all critical conserved active-site residues, fail to exhibit DGC activity in biochemical assays.[25,26] Such enzymes might exhibit conditional DGC activity in the presence of specific endogenous activators.

Conclusion

Our results demonstrate the complex interplay between synthetic small molecules and the regulatory mechanism that drives DGC activation. In many prokaryotic model systems, c-di-GMP-mediated biofilm formation is regulated by multiple DGC enzymes in parallel. Thus our studies underline the importance of in-detail mechanism-of-action studies of candidate

DGC inhibitors prior to their phenotypic evaluation. In the future, it will be interesting to investigate whether distinct fragments of the compounds identified will act as general DGC modulators or exhibit specificity towards distinct DGC subtypes. Compounds that act specifically on distinct enzymes might serve as exciting chemical genetics tools for the dissection of DGC networks, whereas inhibitors with generalized effects of DGC activity might have the potential to serve as lead compounds for the development of biofilm modulators and other c-di-GMP-mediated phenotypes involved in bacterial pathogenesis.

Experimental Section

Compound library: Compounds for screening were provided by the national screening laboratory NSRB, in collaboration with the ICCB-Longwood screening facility located at Harvard Medical School. The chemical library screened is a subset of a compilation of commercially available small-molecule chemical libraries maintained at the ICCB. The compounds have been prescreened for drug-like properties (Lipinski's rules).[27] Stock libraries were stored at a concentration of 5 mg mL^{-1} in DMSO at −80 °C in 384-well format, with at least two empty columns on each plate to allow for on-plate controls. Libraries (number of molecules) from the following companies were evaluated: Asinex Corporation (12377, www.asinex.com, Winston-Salem, NC, USA), Enamine, Ltd. (11264, www.enamine.net, Kiev, Ukraine), and Life Chemicals (3893, Burlington, Canada).

Compounds used for dose–response (IC_{50}) assays: For confirmatory assays and dose–response (IC_{50}) assays the following compounds were purchased: from Enamine: **1** (T5267517), **1a** (T5382986), **1b** (T5423966), **1c** (T5354248), **1d** (T5283214), **1e** (T5290508), **1f** (T5841885), **2g** (T5257569), **2h** (T6309238), **2i** (T5401340), **2k** (T5558380), **2l** (T5555070), **2m** (T5577173), **2n** (T5553390), **2b** (T5577172), **2o** (T6283377), **2p** (T0520-5955), **3** (T5580955), **4** (T5411955); from Asinex: **2** (BAS 05165102), **5** (BAS 01811924), **7** (BAS 14051565), **2c** (BAS 01833594), **2d** (BAS 03310955), **2e** (BAS 03079336), **2j** (BAS 01835812); from ABI Chem (www.abichem.com, Munich, Germany); **6** (AC1N893M), **2a** (AC1LV267); from Molport Corporation (www.molport.com, Riga, Latvia); **2f** (MolPort-002–121–569).

Screening equipment: Multiwell liquid dispensing for setting up assays was performed with the liquid handler PlateMate Plus (Hamilton) and Microflo plate dispenser (Biotek). HTS, DGC enzyme inhibition reactions, and dose–response (IC_{50}) assays were performed in Corning Low Volume 384 Well Black Flat Bottom Polystyrene Microplates (Product #3821BC) in a final volume of 20 μL per well. Change in fluorescence ratio (535/470 nm) was measured with an Envision 2104 fluorescence plate reader (PerkinElmer) to monitor for c-di-GMP production. The plate reader was equipped with a CFP excitation filter (λ_{ex} = 430 nm, BW 24 nm, T_{min} 90%) a dichroic mirror module (D450/D505 nm), emission filters for YFP (CWL 535 nm, BW 30 nm, T_{min} 90%) and CFP (CWL 470 nm, BW 24 nm, T_{min} = 90%), and dual PMT detectors for recording CFP and YFP signals simultaneously. Measurement mode was bi-directional by rows (excitation and emission light set to 100% and number of flashes to 10) with use of dual detector mode with a PMT gain of 383 (535 nm) and 572 (470 nm) and a measurement height of 7 mm above the plate height.

Protein expression: *Escherichia coli* BL21 (DE3) strain BC1058[9] containing the constitutive active *C. crescentus* DGC (CC3285) cloned into pET42b plasmid was used for recombinant expression of the DGC enzyme. DgcA protein was overexpressed and His-tag purified according to ref. [9]. *E. coli* BL21 (DE3) strain containing pET15b::mCPet-12AA-mYPet plasmid was used for recombinant expression of the c-di-GMP biosensor. The expression vector used for protein purification of c-di-GMP biosensors was a modified variant of the pET15b::mCPet-12AA-mYPet[28] containing an N-terminal polyhistidine tag for affinity purification, monomerizing mutations in CYPet (A206K) and YPet (A206K), and a multiple cloning site in its 12-amino-acid linker region between the mYPet and mCYPet FRET pair. Two restriction sites (SpeI and KpnI) were introduced by PCR onto the 5′- and 3′-ends of a codon-optimized version of *Salmonella enterica* serovar Typhimurium ycgR (STM1798) gene, and the products were cloned in-frame into the SpeI and KpnI sites of pET15b::mCPet-12AA-mYPet.[10] YcgR biosenso was overexpressed and His-tag purified according to ref. [9].

Storage of proteins and reagents: All proteins used in our assays were purified by affinity chromatography followed by gel filtration. These enzymes were kept at a low concentration (< 0.1 mg mL^{-1} to prevent aggregation) in a solution containing glycerol (20%), protease inhibitors, and β-mercaptoethanol. The DGC enzyme is active for at least two weeks at 4 °C and > 90% active for at least 48 h at room temperature. The YcgR biosensor can be stably kept for weeks in the dark at 4 °C. For long-term storage the biosensor was stored at −80 °C, in small aliquots containing glycerol (20%), tris buffer (pH 8, 10 mM), and NaCl (250 mM). We have tested biosensor that has been frozen for more than one year for stability and it did not show any significant loss of activity. C-di-GMP is kept at −20 °C for long-term storage as a lyophilized powder or solution. Our current stocks are made in house biosynthetically, by using a constitutive active derivative of DgcA enzyme,[9] and purified by HPLC. GTP stock solutions are prepared just before the assay or screening because it will hydrolyze over time.

Diguanylate cyclase assay: DGC reactions were performed at 25 °C with purified hexahistidine-tagged DgcA (20 nM) and hexahistidine-tagged mCPet-YcgR-mYPet biosensor (50 nM) to monitor change in fluorescence upon c-di-GMP production. The DGC reaction buffer contained NaCl (250 mM), Tris·Cl (pH 8.0, 25 mM), and $MgCl_2$ (20 mM). For screening assays, the reaction mixture was preincubated with compound (200 nL, 5 mg mL^{-1}) in DMSO, and fluorescence emission was measured prior to addition of YcgR biosensor, then again after addition of GTP (t = 0 min), and 3 h post GTP addition as the endpoint measurement. For IC_{50} inhibition assays, the protein was preincubated with different concentrations of compounds dissolved in DMSO (1–100 μM, 1% final DMSO concentration) for 2 min at 25 °C, after which GTP substrate was added to a final concentration of 20 μM. During screening, the fluorescence emission ratio was measured prior to addition of the YcgR biosensor to monitor background fluorescence at 470 and 535 nm. Plates were directly measured after addition of GTP (20 μM, t = 0 min) and then after 3 h incubation at RT. During secondary assays and IC_{50} inhibition assays change in fluorescence ration was measured at time intervals of 1 min. We determined the plate uniformity, signal variability, and repeatability assessment by use of NCGC guidelines. The data were analyzed by using the Excel file supplied by the NCGC assay validation website. We conducted the "plate uniformity assay" recommended by NCGC for CV and Z factor calculation for measuring plate-to-plate variation as well as day-to-day variation. The average Z factor for three plates, read on two

consecutive days, was 0.71 and the CV for high, medium, and low signal were well below 5%.

Data analysis: Data analysis was performed in Excel 97. All primary screening was performed at 50 μg mL^{-1} compound concentrations. The fluorescence emission ratio (535/470 nm) of the YcgR biosensor in the absence of c-di-GMP was used as the positive control for DgcA inhibition; biosensor in the presence of c-di-GMP (5 μM) served as the negative control. For a compound to be considered a hit, the following criteria had to be met: 1) compounds with c-di-GMP levels below 300 nM after 3 h incubation with DgcA and GTP (20 μM) were considered strong hits, 2) duplicates had to be consistent, with difference in final c-di-GMP levels $<$100 nM, and 3) background fluorescence prior to addition of the FRET biosensor could not exceed 7% of the FRET signal in CFP and YFP emission channels. Total fluorescence was used as a quality control criterion to identify inherently fluorescent molecules. Of the 27502 compounds screened in duplicate, 1029 (3.7%) were removed from the analysis due to autofluorescence, and 49 compounds (0.19%) exhibited c-di-GMP levels below 300 nM after 3 h incubation with DgcA enzyme. Of these, 18 compounds were tested in secondary assays. Seven had potencies below 50 μM and three compounds below 10 μM.

The FRET fluorescence emission ratio was defined as [Eq. (1)]:

$$\mathrm{FRET} = \frac{\mathrm{Em}_{527\,\mathrm{nm}}}{\mathrm{Em}_{470\,\mathrm{nm}}} \tag{1}$$

The following formula involving the means of the FRET ratios of positive and negative controls (μ_+, μ_-) and their standard deviations (σ_+, σ_-) was used to calculate the Z' factor of the FRET-based HTS assay [Eq. (2)]:

$$Z'\ \mathrm{factor} = 1 - \frac{3\sigma_+ + 3\sigma_-}{|\mu_+ - \mu_-|} \tag{2}$$

Θ, the fraction of YcgR biosensor in the c-di-GMP bound state, was calculated according to [Eq. (3)]:

$$\Theta = \frac{\mathrm{FRET}_{\mathrm{free}} - \mathrm{FRET}_{\mathrm{assay}}}{\mathrm{FRET}_{\mathrm{free}} - \mathrm{FRET}_{\mathrm{bound}}} \tag{3}$$

where $\mathrm{FRET}_{\mathrm{free}}$ is the fluorescence emission ratio (535/470 nm) of the free biosensor, $\mathrm{FRET}_{\mathrm{bound}}$ is the fluorescence emission ratio (535/470 nm) of YcgR with c-di-GMP bound, and $\mathrm{FRET}_{\mathrm{assay}}$ is the fluorescence emission ratio (535/470 nm) of the YcgR biosensor during the assay.

The c-di-GMP concentration (in nM) was calculated according to [Eq. (4)]:

$$[\text{c-di-GMP}] = \sqrt{\frac{\Theta {K_D}^2}{1-\Theta}} \tag{4}$$

with K_D = 198 nM, c-di-GMP dissociation constant of the YcgR biosensor at 25 °C.

Initial velocity (V_0) was determined by plotting c-di-GMP concentration versus time and by fitting the curve according to Michaelis–Menten kinetics. The dose–response curves of percentage activity were fit in ProFit 5.6.7.

IC_{50} inhibition constants were fitted by using the following function [Eq. (5)]:

$$A(I) = A_{ES} - \frac{[(A_{ES} - A_{ESI})[I]]^{\eta}}{IC_{50}^{\eta} + [I]^{\eta}} \tag{5}$$

where $A(I)$ = relative DGC enzymatic activity as a function of inhibitor concentration, A_{ES} = relative activity in absence of inhibitor, A_{ESI} = relative residual activity under inhibitor saturating conditions, IC_{50} = half-maximum inhibitory concentration of inhibitor, [I] concentration of inhibitor, and η = Hill coefficient.

AC_{50} constants were fitted with the following function [Eq. (6)]:

$$A(I) = A_{ES} + \frac{[(A_{ESI} - A_{ES})[I]]^{\eta}}{AC_{50}^{\eta} + [I]^{\eta}} \tag{6}$$

where $A(I)$ = relative DGC enzymatic activity as a function of activator concentration, A_{ES} = relative activity in absence of activator, A_{ESI} = relative activity under activator saturating conditions, AC_{50} = half-maximum activating concentration of activator, [I] = concentration of activator, and η = Hill coefficient.

All hit validation and HTS procedures were carried out according to the general guidelines as published on the U.S. National Chemical Genomics Center web site (NCGC Assay Guidance Manual and High-Throughput Assay Guidance criteria, http://www.ncbi.nlm.nih.gov/books/NBK53196/).

Chemistry

General methods: All reactions were run under dry nitrogen. Reagents and solvents were obtained in the highest available purity and used without further purification unless indicated. ^{1}H NMR and ^{13}C NMR spectra were obtained with a 500 MHz (Bruker AV500) instrument. Identities of the compounds were confirmed by mass spectrometry. A solution of each compound was infused into the electrospray ionization source operating in positive- or negative-ion mode. Low-resolution spectra were obtained with an Esquire LC ion trap mass spectrometer (Bruker Daltonics, Billerica, MA). Accurate mass measurements were performed with an APEX Qe 47 Fourier transform ion cyclotron resonance mass spectrometer (Bruker Daltonics). Normal-phase silica gel purifications were performed with a Biotage SP4 instrument and the cartridges supplied by Biotage. RP-HPLC was carried out with a Varian instrument equipped with a diode array ultraviolet detector. For preparative reversed-phase chromatography a 10×250 mm C_{18} 5μ column at a flow rate of 4.6 mL min^{-1} was used; for analytical reversed-phase chromatography a 4.6×250 mm C_{18} 5μ column at a flow rate of 1 mL min^{-1} was used. Ultraviolet detection was at 215 and either 254 or 360 nm. Unless otherwise specified, buffer A was trifluoroacetic acid (TFA) in H_2O (0.05%), whereas buffer B was TFA in acetonitrile (0.05%). Thin-layer chromatography was performed with 0.2 mm polygram SIL G/UV plates (Alltech, Deerfield, IL), developed with mobile phases of varying compositions of ethyl acetate/hexane, MeOH/CH_2Cl_2, or MeOH/$CHCl_3$, and visualized by UV light supplemented by vanillin, ninhydrin, and other solution stains where appropriate.

1-[2-(Benzyloxy)acetyl]pyrrolidin-2-one (1w; Scheme 1): 1-(Trimethylsilanyl)pyrrolidin-2-one (5.9 mL, 36.95 mmol) in diethyl ether (55 mL) was added dropwise at 0 °C to a solution of benzyloxyacetyl chloride (5.3 mL, 33.59 mmol) in diethyl ether (55 mL). The ice bath was removed, and the reaction mixture was stirred at room temperature 1.5 h and then concentrated in vacuo. The crude product was purified by silica gel chromatography with a gradient of ethyl acetate in hexanes (30 to 60%) to give **1w** (7.425 g, 31.87 mmol). ^{1}H NMR (500 MHz, $CDCl_3$): δ = 1.92–2.08 (m, 2H), 2.48 (td, J = 8.0, 3.6 Hz, 2H), 3.75 (td, J = 7.0, 3.7 Hz, 2H), 4.61 (s, 4H),

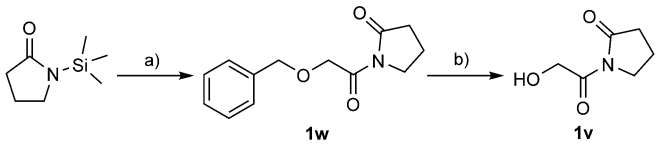

Scheme 1. Synthesis of **1 v**. a) Benzyloxyacetyl chloride, diethyl ether, 0 °C–RT, 1.5 h. b) H_2, Pd-C, EtOH, DMF.

7.15–7.28 (m, 1H), 7.29 (t, J = 6.6 Hz, 2H), 7.32–7.49 ppm (m, 2H); ^{13}C NMR (500 MHz, $CDCl_3$): δ = 17.74, 33.00, 44.78, 70.83, 73.21, 127.79, 127.94, 128.37, 137.53, 171.16, 175.70 ppm; MS: *m/z*: 256.2 $[M+Na]^+$.

1-(2-Hydroxyacetyl)pyrrolidin-2-one (1 v): In a flame-dried flask, EtOH (200 mL) was bubbled with argon for 10 min. Palladium on carbon (10%, 7.425 g) was added, and the suspension was bubbled with argon for 10 min, **1 w** (7.425 g, 31.87 mmol) in EtOH (100 mL) and DMF (33 mL) was then added, and the system was bubbled with argon for 10 min and then with H_2 until completion. The solution was bubbled with argon for a further 10 min, filtered through celite, and concentrated in vacuo to give **1 v** (4.436 g, 31.02 mmol). ^{1}H NMR (500 MHz, $CDCl_3$): δ = 2.05–2.20 (m, 2H), 2.58 (t, J = 8.1 Hz, 2H), 3.83 (t, J = 7.2 Hz, 2H), 4.62 ppm (s, 2H); ^{13}C NMR (500 MHz, $CDCl_3$): δ = 17.91, 32.88, 44.93, 64.17, 174.30, 175.92 ppm; MS: *m/z*: 166.1 $[M+Na]^+$; HRMS: *m/z* calcd for $C_7H_{13}NNaO_4$ $[M+Na+CH_3OH]^{+1}$: 198.0737; found: 198.0736.

2-Oxo-2-(2-oxopyrrolidin-1-yl)ethyl 2-methylbenzo[d]thiazole-6-carboxylate (1 i)—General Method A (Scheme 2): *N*′-(3-Dimethylaminopropyl)-*N*-ethylcarbodiimide (EDCI, 131 mg, 0.44 mmol), 4-dimethylaminopridine (DMAP, 3 mg, 0.027 mmol), and 2-methyl-1,3-benzothiazole-6-carboxylic acid (55 mg, 0.31 mmol) were added to a solution of **1 v** (49 mg, 0.34 mmol) in CH_2Cl_2 (2 mL) and DMF (0.5 mL). The reaction mixture was stirred at room temperature overnight and then partitioned between CH_2Cl_2 and saturated $NaHCO_3$ solution. The organic layer was washed with brine, dried over Na_2SO_4, filtered, and concentrated in vacuo. The crude product was purified by silica gel chromatography with a gradient of MeOH in CH_2Cl_2 (0 to 3%) to give **1 i** (62 mg, 0.19 mmol). ^{1}H NMR (500 MHz, $CDCl_3$): δ = 2.08–2.21 (m, 2H), 2.62 (t, J = 8.1 Hz, 2H), 2.86 (s, 3H), 3.83 (t, J = 7.2 Hz, 2H), 5.42 (s, 2H), 7.98 (d, J = 8.6 Hz, 1H), 8.18 (dd, J = 8.6, 1.7 Hz, 1H), 8.62 ppm (d, J = 1.3 Hz, 1H); ^{13}C NMR (500 MHz, $CDCl_3$): δ = 17.89, 20.46, 32.91, 44.87, 65.01, 122.16, 124.06, 125.84, 127.55, 135.65, 156.58, 165.70, 167.92, 171.06, 176.09 ppm; MS: *m/z*: 341.5 $[M+Na]^+$; HRMS: *m/z* calcd for $C_{15}H_{14}N_2NaO_4S$ $[M+Na]^+$: 341.0566; found: 341.0569.

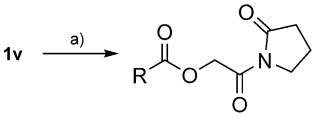

Scheme 2. General method A. a) 2-Methylbenzo[d]thiazole-5-carboxylic acid, EDCI, DMAP, CH_2Cl_2, DMF, RT, overnight.

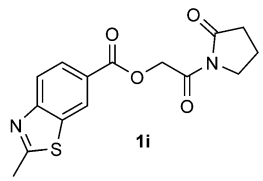

2-Oxo-2-(2-oxopyrrolidin-1-yl)ethyl benzo[d]oxazole-6-carboxylate (1 g): Compound **1 g** was prepared according to the procedure in General Method A from **1 v** and benzo[d]oxazole-6-carboxylic acid on a 0.30 mmol scale. The crude product was purified five times by silica gel chromatography with a gradient of MeOH in CH_2Cl_2 (0 to 5%) to give **1 g** (25 mg, 0.087 mmol). ^{1}H NMR (500 MHz, $CDCl_3$): δ = 2.08–2.26 (m, 2H), 2.66 (t, J = 8.1 Hz, 2H), 3.87 (t, J = 7.2 Hz, 2H), 5.45 (s, 2H), 7.86 (d, J = 8.3 Hz, 1H), 8.19 (d, J = 8.3 Hz, 1H), 8.26 (s, 1H), 8.38 ppm (s, 1H); ^{13}C NMR (500 MHz, $CDCl_3$): δ = 17.92, 32.93, 44.89, 65.13, 113.21, 120.40, 126.67, 127.15, 144.15, 149.65, 155.06, 165.56, 167.86, 176.13 ppm; MS: *m/z*: 311.2 $[M+Na]^+$; HRMS: *m/z* calcd for $C_{14}H_{12}N_2NaO_5$ $[M+Na]^+$: 311.0638; found: 311.0644.

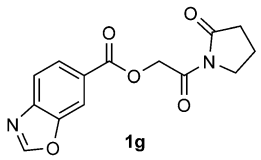

2-Oxo-2-(2-oxopyrrolidin-1-yl)ethyl benzofuran-5-carboxylate (1 j): Compound **1 j** was prepared according to the procedure in General Method A from **1 v** and benzofuran-5-carboxylic acid on a 0.38 mmol scale. The crude product was purified by silica gel chromatography with a gradient of MeOH in CH_2Cl_2 (0 to 5%) to give **1 j** (23.6 mg, 0.082 mmol). ^{1}H NMR (500 MHz, $CDCl_3$): δ = 2.09–2.27 (m, 2H), 2.66 (t, J = 8.1 Hz, 2H), 3.87 (t, J = 7.2 Hz, 2H), 5.45 (s, 2H), 6.87 (d, J = 1.2 Hz, 1H), 7.57 (d, J = 8.7 Hz, 1H), 7.72 (d, J = 2.0 Hz, 1H), 8.12 (dd, J = 8.7, 1.4 Hz, 1H), 8.45 ppm (s, 1H); ^{13}C NMR (500 MHz, $CDCl_3$): δ = 17.92, 32.97, 44.90, 64.87, 107.17, 111.37, 124.25, 124.43, 126.44, 127.49, 146.31, 157.71, 166.30, 168.17, 176.09 ppm; MS: *m/z*: 310.3 $[M+Na]^+$; HRMS: *m/z* calcd for $C_{15}H_{13}NNaO_5$ $[M+Na]^+$: 310.0686; found: 310.0690.

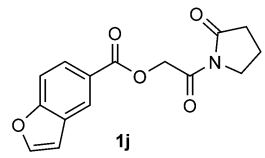

2-Oxo-2-(2-oxopyrrolidin-1-yl)ethyl 1*H*-indole-5-carboxylate (1 k): Compond **1 k** was prepared according to the procedure in General Method A from **1 v** and 1*H*-indole-5-carboxylic acid on a 0.29 mmol scale. The crude product was purified four times by silica gel chromatography with a gradient of ethyl acetate in hexanes (10 to 50%) to give **1 k** (8.2 mg, 0.029 mmol). ^{1}H NMR (500 MHz, [D_7]DMF): δ = 2.26–2.45 (m, 2H), 2.85 (t, J = 8.1 Hz, 2H), 3.97 (t, J = 7.2 Hz, 2H), 5.59 (s, 2H), 6.88 (s, 1H), 7.70–7.89 (m, 2H), 8.04 (dd, J = 8.6, 1.4 Hz, 1H), 8.60 (s, 1H), 11.77 ppm (s, 1H); ^{13}C NMR (500 MHz, [D_7]DMF): δ = 17.87, 32.82, 45.05, 64.50, 103.02, 111.61, 120.70, 122.60, 123.51, 127.52, 127.98, 139.46, 166.96, 168.32, 176.78 ppm; MS: *m/z*: 309.2 $[M+Na]^+$; HRMS: *m/z* calcd for $C_{15}H_{14}N_2NaO_4$ $[M+Na]^+$: 309.0846; found: 309.0837.

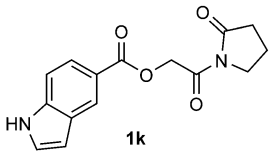

2-Oxo-2-(2-oxopyrrolidin-1-yl)ethyl 1-methyl-1*H*-indole-5-carboxylate (1 l): Compound **1 l** was prepared according to the procedure in General Method A from **1 v** and 1-methyl-1*H*-indole-5-carboxylic acid on a 0.39 mmol scale. The crude product was purified three times by silica gel chromatography with a gradient of MeOH in CH_2Cl_2 (0 to 3%) to give **1 l** (6.3 mg, 0.021 mmol). ^{1}H NMR

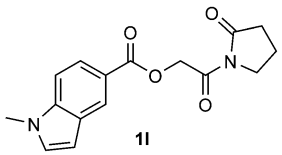

1l

(500 MHz, $CDCl_3$): δ = 2.10–2.26 (m, 2H), 2.67 (t, J = 8.1 Hz, 2H), 3.86 (s, 3H), 3.89 (t, J = 7.2 Hz, 2H), 5.44 (s, 2H), 6.62 (d, J = 3.0 Hz, 1H), 7.14 (d, J = 3.2 Hz, 1H), 7.37 (d, J = 8.7 Hz, 1H), 8.02 (dd, J = 8.7, 1.4 Hz, 1H), 8.51 ppm (s, 1H); ^{13}C NMR (500 MHz, $CDCl_3$): δ = 17.93, 33.02, 33.07, 44.91, 64.64, 102.78, 108.90, 120.53, 123.31, 124.51, 128.00, 130.26, 139.36, 167.25, 168.55, 176.04 ppm; MS: m/z: 323.2 $[M+Na]^+$; HRMS: m/z calcd for $C_{17}H_{20}N_2NaO_5$ $[M+Na+CH_3OH]^{+1}$: 355.1264; found: 355.1258.

2-Oxo-2-(2-oxopyrrolidin-1-yl)ethyl 1-methyl-1*H*-benzo[d]imidazole-5-carboxylate (1 m): Compound **1 m** was prepared according

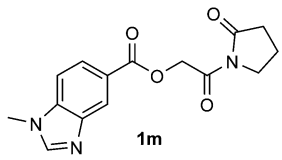

1m

to the procedure in General Method A from **1 v** and 1-methyl-1*H*-benzimidazole-5-carboxylic acid on a 0.36 mmol scale under argon. The crude product was purified twice by silica gel chromatography with a gradient of MeOH in CH_2Cl_2 (0 to 15%) to give **1 m** (4 mg, 0.013 mmol). ^{1}H NMR (500 MHz, $CDCl_3$): δ = 2.11–2.28 (m, 2H), 2.68 (t, J = 8.1 Hz, 2H), 3.81–4.03 (m, 5H), 5.47 (s, 2H), 7.46 (d, J = 8.5 Hz, 1H), 7.99 (s, 1H), 8.15 (dd, J = 8.5, 1.3 Hz, 1H), 8.64 ppm (s, 1H); ^{13}C NMR (500 MHz, $CDCl_3$): δ = 17.94, 31.28, 33.00, 44.91, 64.88, 109.15, 123.35, 123.65, 124.93, 138.01, 143.40, 145.29, 166.64, 168.25, 176.05 ppm; MS: m/z: 302.2 $[M+H]^+$; HRMS: m/z calcd for $C_{15}H_{16}N_3O_4$ $[M+H]^+$: 302.1135; found: 302.1142.

2-Oxo-2-(2-oxopyrrolidin-1-yl)ethyl isoquinoline-6-carboxylate (1 n): Compound **1 n** was prepared according to the procedure in General Method A from **1 v** and isoquinoline-6-carboxylic acid on a 0.36 mmol scale. The crude product was purified four times by silica gel chromatography with a gradient of MeOH in CH_2Cl_2 (0 to 10%) to give **1 n** (6.4 mg, 0.021 mmol). ^{1}H NMR (500 MHz, $CDCl_3$): δ = 2.13–2.31 (m, 2H), 2.69 (t, J = 8.1 Hz, 2H), 3.90 (t, J = 7.1 Hz, 2H), 5.52 (s, 2H), 7.80 (d, J = 5.3 Hz, 1H), 8.09 (d, J = 8.5 Hz, 1H), 8.27 (d, J = 8.4 Hz, 1H), 8.65 (d, J = 5.3 Hz, 1H), 8.70 (s, 1H), 9.39 ppm (s, 1H); ^{13}C NMR (500 MHz, $CDCl_3$): δ = 17.95, 32.94, 44.91, 65.27, 121.45, 126.98, 128.04, 129.96, 130.90, 135.02, 143.91, 152.57, 165.55, 167.74, 176.15 ppm; MS: m/z: 321.3 $[M+Na]^+$; HRMS: m/z calcd for $C_{16}H_{15}N_2O_4$ $[M+H]^+$: 299.1026; found: 299.1027.

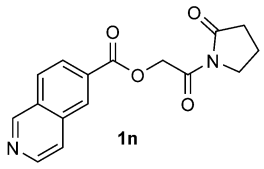

1n

2-Oxo-2-(2-oxopyrrolidin-1-yl)ethyl quinoxaline-6-carboxylate (1 o): Compound **1 o** was prepared according to the procedure in General Method A from **1 v** and quinoxaline-6-carboxylic acid on a 0.37 mmol scale. The crude product was purified by silica gel chromatography with a gradient of MeOH in CH_2Cl_2 (0 to 10%) to give **1 o** (20.6 mg, 0.069 mmol). ^{1}H NMR (500 MHz, $CDCl_3$): δ = 2.08–2.29 (m, 2H), 2.67 (t, J = 7.6 Hz, 2H), 3.88 (t, J = 6.2 Hz, 2H), 5.51 (s, 2H), 8.20 (d, J = 8.4 Hz, 1H), 8.44 (d, J = 8.1 Hz, 1H), 8.86–9.06 ppm (m, 3H); ^{13}C NMR (500 MHz, $CDCl_3$): δ = 17.94, 32.92, 44.90, 65.35, 129.75, 129.93, 130.77, 132.80, 142.30, 145.15, 146.01, 146.75, 165.24, 167.64, 176.14 ppm; MS: m/z: 322.3 $[M+Na]^+$; HRMS: m/z calcd for $C_{15}H_{13}N_3NaO_4$ $[M+Na]^+$: 322.0798; found: 322.0790.

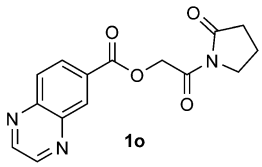

1o

2-Oxo-2-(2-oxopyrrolidin-1-yl)ethyl benzothiazole-5-carboxylate (1 p): Compound **1 p** was prepared according to the procedure in General Method A from **1 v** and benzothiazole-5-carboxylic acid on a 0.36 mmol scale. The crude product was purified by silica gel chromatography with a gradient of MeOH in CH_2Cl_2 (0 to 3%) to give **1 p** (43.7 mg, 0.14 mmol). ^{1}H NMR (500 MHz, $CDCl_3$): δ = 2.06–2.25 (m, 2H), 2.64 (t, J = 8.1 Hz, 2H), 3.85 (t, J = 7.2 Hz, 2H), 5.46 (s, 2H), 8.03 (d, J = 8.4 Hz, 1H), 8.18 (d, J = 7.6 Hz, 1H), 8.88 (s, 1H), 9.09 ppm (s, 1H); ^{13}C NMR (500 MHz, $CDCl_3$): δ = 17.91, 32.93, 44.89, 65.11, 121.93, 125.64, 126.36, 127.86, 138.91, 153.13, 155.39, 165.85, 167.86, 176.13 ppm; MS: m/z: 327.3 $[M+Na]^+$; HRMS: m/z calcd for $C_{14}H_{12}N_2NaO_4S$ $[M+Na]^+$: 327.0410; found: 327.0407.

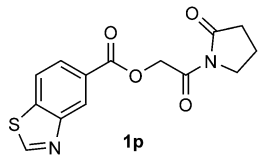

1p

1-(2-Bromoacetyl)pyrrolidin-2-one (1 x; Scheme 3): Carbon tetrabromide (126 mg, 0.38 mmol) was added at 0 °C to a solution of **1 v** (50 mg, 0.35 mmol) in CH_2Cl_2 (1 mL). A solution of triphenylphosphine (100 mg, 0.38 mmol) in CH_2Cl_2 (0.5 mL) was added dropwise and the reaction mixture was allowed to warm to room temperature overnight. The crude reaction mixture was concentrated in vacuo and purified by silica gel chromatography with a gradient of MeOH in CH_2Cl_2 (0 to 5%) to give **1 x** (48 mg, 0.23 mmol). ^{1}H NMR (500 MHz, $CDCl_3$): δ = 2.05–2.17 (m, 2H), 2.65 (t, J = 8.1 Hz, 2H), 3.86 (t, J = 7.3 Hz, 2H), 4.50 ppm (s, 2H); ^{13}C NMR (500 MHz, $CDCl_3$): δ = 17.35, 30.09, 33.11, 45.82, 166.61, 175.38 ppm; MS: m/z: 230.2 $[M+Na]^+$; HRMS: m/z calcd for $C_7HBrNNaO_3$ $[M+Na+CH_3OH]^{+1}$: 259.9893; found: 259.9892.

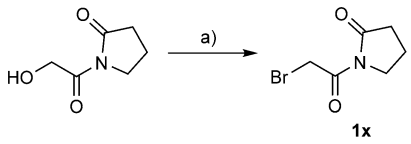

1x

Scheme 3. Synthesis of **1 x**. a) CBr_4, triphenylphosphine, CH_2Cl_2, RT, overnight.

Benzyl-(2-oxo-2-(2-oxopyrrolidin-1-yl)ethyl)carbamate (1 y; Scheme 4): PCl_5 (458 mg, 2.2 mmol) was added at −15 °C to a solution of Cbz-Gly (418 mg, 2.0 mmol) in diethyl ether (2.5 mL). The reaction mixture was stirred for 3 h at 0 °C, and then concentrated in vacuo. The crude acid chloride was taken up in diethyl ether (3.5 mL), and 1-(trimethylsilanyl)pyrrolidin-2-one (0.35 mL, 2.2 mmol) in diethyl ether (3.5 mL) was added dropwise at 0 °C. The ice bath was removed and the reaction mixture was stirred at room temperature for 1.25 h and then concentrated in vacuo. The crude product was partitioned between ethyl acetate and $NaHCO_3$

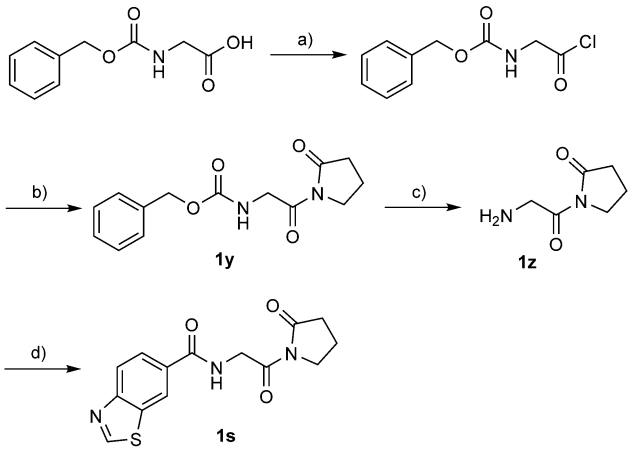

Scheme 4. Synthesis of **1 s**. a) PCl_5, diethyl ether, −15 to 0 °C, 3 h; b) 1-(trimethylsilanyl)pyrrolidin-2-one, diethyl ether, 0 °C–RT, 1.25 h; c) TFA, thioanisole, TMSBr, RT, 1.5 h; d) benzothiazole-6-carboxylic acid, HBTU, HOAt, DIEA, DMF, CH_2Cl_2, RT, overnight.

solution (10%). The aqueous fraction was reextracted three times with ethyl acetate, and the combined organic extracts were washed with brine, dried over Na_2SO_4, filtered, and concentrated in vacuo. The crude product was purified by silica gel chromatography with a gradient of MeOH in CH_2Cl_2 (0 to 10%) to give **1 y** (369 mg, 1.34 mmol). ^{1}H NMR (500 MHz, $CDCl_3$): δ = 1.85–2.07 (m, 2H), 2.47 (t, J = 8.1 Hz, 2H), 3.68 (t, J = 7.2 Hz, 2H), 4.42 (d, J = 5.6 Hz, 2H), 5.05 (s, 2H), 5.88 (br t, J = 5.2 Hz, 1H), 7.15–7.50 ppm (m, 5H); ^{13}C NMR (500 MHz, $CDCl_3$): δ = 17.52, 33.01, 45.10, 46.33, 66.72, 127.96, 128.29, 136.56, 156.56, 170.39, 175.85 ppm; MS: *m/z*: 299.3 $[M+Na]^+$.

1-(2-Aminoacetyl)pyrrolidin-2-one (1 z): Thioanisole (4.0 mL, 33.88 mmol) and TMSBr (0.89 mL, 6.78 mmol) were added to a solution of **1 y** (187 mg, 0.68 mmol) in TFA (13.5 mL). The reaction mixture was stirred at room temperature for 1.5 h and then concentrated in vacuo. The crude product was purified by silica gel chromatography with a gradient of MeOH in CH_2Cl_2 (0 to 25%) to give **1 z**, which was used without further purification. ^{1}H NMR (500 MHz, MeOD): δ = 2.08–2.25 (m, 2H), 2.33 (t, J = 8.1 Hz, 1H), 2.66 (t, J = 8.1 Hz, 1H), 3.43 (t, J = 7.0 Hz, 1H), 3.77–3.94 (m, 3H), 4.35 ppm (br s, 2H); ^{13}C NMR (500 MHz, MeOD): δ = 17.23, 32.31, 42.30, 44.88, 167.37, 177.17 ppm; MS: *m/z*: 143.2 $[M+H]^+$.

***N*-(2-Oxo-2-(2-oxopyrrolidin-1-yl)ethyl)benzo[d]thiazole-6-carboxamide (1 s)**: A solution of benzothiazole-6-carboxylic acid (122 mg, 0.68 mmol), *N*-[(1*H*-benzotriazole-1-yl)(dimethylamino)-methylene]-*N*-methylmethanaminium hexafluorophosphate *N*-oxide (HBTU, 774 mg, 2.04 mmol), and 1-hydroxy-7-azabenzotriazole (HOAt, 278 mg, 2.04 mmol) in CH_2Cl_2 (5 mL) and DMF (1 mL) was stirred at room temperature for 1 h, **1 z** (96 mg, 0.68 mmol) and *N*,*N*′-diisopropylethylamine (DIEA, 0.53 mL, 3.04 mmol) in DMF (2 mL) were then added, and the reaction mixture was stirred overnight. The reaction mixture was diluted with CH_2Cl_2 and washed with water and saturated $NaHCO_3$ solution, dried over Na_2SO_4, filtered, and concentrated in vacuo. The crude product was purified by reversed-phase HPLC with a gradient from 10 to 95% B in A over 30 min to give **1 s** (20.5 mg, 0.068 mmol). ^{1}H NMR (500 MHz, $CDCl_3$): δ = 2.10–2.25 (m, 2H), 2.67 (t, J = 8.1 Hz, 2H), 3.89 (t, J = 7.2 Hz, 2H), 4.84 (d, J = 5.1 Hz, 2H), 7.25 (br s, 1H), 7.97 (dd, J = 8.5, 1.6 Hz, 1H), 8.18 (d, J = 8.5 Hz, 1H), 8.53 (d, J = 1.4 Hz, 1H), 9.18 ppm (s, 1H); ^{13}C NMR (500 MHz, $CDCl_3$): δ = 17.67, 33.09, 45.21, 45.67, 121.99, 123.42, 124.98, 131.42, 134.03, 154.79, 157.08, 166.87, 170.01, 175.71 ppm; MS: *m/z*: 304.4 $[M+H]^+$; HRMS: *m/z* calcd for $C_{14}H_{14}N_3O_3S$ $[M+H]^+$: 304.0750; found: 304.0751.

1-(2-Bromopropanoyl)pyrrolidin-2-one (1 aa; Scheme 5): A solution of 1-(trimethylsilanyl)pyrrolidin-2-one (168 μL, 1.05 mmol) in diethyl ether (2 mL) was added dropwise and quickly at 0 °C to a

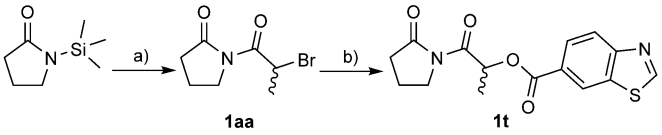

Scheme 5. Synthesis of **1 t**. a) 2-bromopropionyl bromide, diethyl ether, 0 °C–RT, 1.25 h; b) Benzothiazole-6-carboxylic acid, Cs_2CO_3, DMF, RT, overnight.

solution of 2-bromopropionyl bromide (100 μL, 0.95 mmol) in diethyl ether (2 mL). The ice bath was removed and the reaction mixture was stirred at room temperature for 1.25 h and then concentrated in vacuo. The residue was partitioned between ethyl acetate and $NaHCO_3$ (10%). The aqueous layer was reextracted three times with ethyl acetate, and the combined organic layers were washed with brine, dried over Na_2SO_4, filtered, and concentrated in vacuo to give **1 aa** (191.7 mg, 0.87 mmol), which was used without further purification. ^{1}H NMR (500 MHz, $CDCl_3$): δ = 1.76 (d, J = 6.8 Hz, 3H), 1.99–2.10 (m, 2H), 2.53–2.67 (m, 2H), 3.71–3.89 (m, 2H), 5.63 ppm (q, J = 6.8 Hz, 1H); ^{13}C NMR (500 MHz, $CDCl_3$): δ = 17.05, 20.62, 33.51, 40.44, 46.03, 170.29, 174.92 ppm; MS: *m/z*: 244.0 $[M+Na]^+$.

1-Methyl-2-oxo-2-(2-oxopyrrolidin-1-yl)ethyl benzothiazole-6-carboxylate (1 t): Benzothiazole-6-carboxylic acid (156 mg, 0.87 mmol) and cesium carbonate (311 mg, 0.95 mmol) were added to a solution of **1 aa** (192 mg, 0.87 mmol) in DMF (4 mL). The reaction mixture was stirred overnight to completion and was partitioned between H_2O and CH_2Cl_2. The aqueous layer was re-extracted twice with CH_2Cl_2, and the combined organic layers were washed with brine, dried over Na_2SO_4, filtered, and concentrated in vacuo. The crude product was purified by silica gel chromatography with a gradient of EtOAc in hexanes (40 to 60%) to give **1 t** (184 mg, 0.58 mmol). ^{1}H NMR (500 MHz, $CDCl_3$): δ = 1.64 (d, J = 6.8 Hz, 3H), 1.96–2.17 (m, 2H), 2.48–2.77 (m, 2H), 3.67–3.98 (m, 2H), 6.20 (q, J = 6.8 Hz, 1H), 8.09–8.27 (m, 2H), 8.71 (d, J = 1.1 Hz, 1H), 9.14 ppm (s, 1H); ^{13}C NMR (500 MHz, $CDCl_3$): δ = 16.63, 17.48, 33.35, 45.45, 70.89, 123.39, 124.52, 126.78, 127.50, 133.74, 156.20, 157.61, 165.56, 171.70, 175.30 ppm; MS: *m/z*: 341.2 $[M+Na]^+$; HRMS: *m/z* calcd for $C_{15}H_{15}N_2O_4S$ $[M+H]^+$: 319.0747; found: 319.0743.

3-*tert*-Butoxy-3-oxopropyl benzo[d]thiazole-6-carboxylate (1 ab; Scheme 6): Compound **1 ab** was prepared according to the procedure in General Method A from *tert*-butyl 3-hydroxypropionate and benzothiazole-6-carboxylic acid on a 1.0 mmol scale. The crude product was purified by silica gel chromatography with a gradient of MeOH in CH_2Cl_2 (0 to 5%) to give **1 ab** (227 mg, 0.74 mmol). ^{1}H NMR (500 MHz, $CDCl_3$): δ = 1.40 (s, 9H), 2.69 (t, J = 6.3 Hz, 2H), 4.56 (t, J = 6.3 Hz, 2H), 8.09 (s, 2H), 8.60 (s, 1H), 9.11 ppm (s, 1H); ^{13}C NMR (500 MHz, $CDCl_3$): δ = 28.02, 35.25, 61.07, 81.04, 123.33, 124.21, 127.20, 127.26, 133.73, 156.02, 157.43, 165.63, 169.80 ppm; MS: *m/z*: 330.3 $[M+Na]^+$.

3-(Benzo[*d*]thiazole-6-carbonyloxy)propanoic acid (1 ac): Compound **1 ab** (227 mg, 0.74 mmol) was dissolved in TFA (3 mL) and CH_2Cl_2 (3 mL), and the mixture was stirred at room temperature for

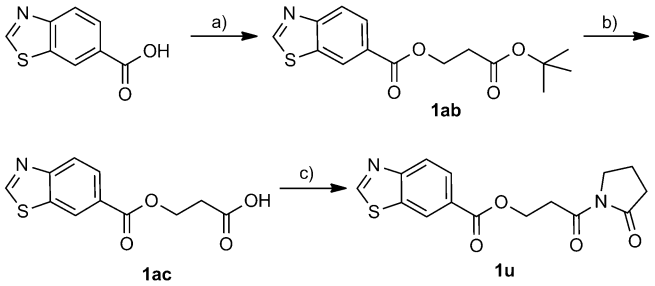

Scheme 6. Synthesis of **1u**. a) *tert*-Butyl 3-hydroxypropionate, EDCI, DMAP, CH_2Cl_2, DMF, RT, overnight; b) H_2, Pd-C, EtOH, DMF, TFA, CH_2Cl_2; c) benzothiazole-6-carboxylic acid, EDCI, DMAP, CH_2Cl_2, DMF, RT, overnight.

2.5 h and concentrated in vacuo to give **1ac** (171 mg, 0.68 mmol), which was used without further purification. ^{1}H NMR (500 MHz, $CDCl_3$): $\delta = 2.94$ (t, $J = 6.0$ Hz, 2H), 4.70 (t, $J = 6.0$ Hz, 2H), 8.21 (s, 2H), 8.73 (s, 1H), 9.22 ppm (s, 1H); MS: *m/z*: 252.3 $[M+H]^+$.

3-Oxo-3-(2-oxopyrrolidin-1-yl)propyl benzo[*d*]thiazole-6-carboxylate (1u): Compound **1ac** (170 mg, 0.68 mmol) was taken up in thionyl chloride (5 mL) with a drop of DMF, stirred at room temperature overnight, and then concentrated in vacuo. The crude acid chloride was taken up in THF (7 mL) and chilled to 0 °C in an ice bath. 1-(Trimethylsilanyl)pyrrolidin-2-one (0.12 mL, 0.75 mmol) in THF (1 mL) was added dropwise quickly, the ice bath was removed, and the reaction mixture was stirred at room temperature for 4 h before concentration in vacuo. The crude product was purified by silica gel chromatography with a gradient of MeOH in CH_2Cl_2 (0 to 5%) to give **1u** (108 mg, 0.34 mmol). ^{1}H NMR (500 MHz, $CDCl_3$): $\delta =$ 1.95–2.13 (m, 2H), 2.59 (t, $J = 8.0$ Hz, 2H), 3.40 (t, $J = 6.2$ Hz, 2H), 3.81 (t, $J = 7.1$ Hz, 2H), 4.69 (t, $J = 6.2$ Hz, 2H), 8.04–8.22 (m, 2H), 8.63 (s, 1H), 9.13 ppm (s, 1H); ^{13}C NMR (500 MHz, $CDCl_3$): $\delta = 17.20$, 33.50, 36.38, 45.34, 60.21, 123.31, 124.27, 127.32, 127.38, 133.70, 156.01, 157.42, 165.79, 170.91, 175.62 ppm; MS: *m/z*: 341.3 $[M+Na]^+$; HRMS: *m/z* calcd for $C_{15}H_{14}N_2NaO_4S$ $[M+Na]^+$: 341.0566; found: 341.0562.

2-Oxo-2-(2-oxopyrrolidin-1-yl)ethyl benzoate (1h): Compound **1h** was prepared according to the procedure in General Method A from **1v** and benzoic acid on a 0.35 mmol scale. The crude product was purified by silica gel chromatography with a gradient of MeOH in CH_2Cl_2 (0 to 3%) to give **1h** (52.1 mg, 0.21 mmol). ^{1}H NMR (500 MHz, $CDCl_3$): $\delta = 2.02$–2.18 (m, 2H), 2.61 (t, $J = 8.1$ Hz, 2H), 3.83 (t, $J = 7.2$ Hz, 2H), 5.40 (s, 2H), 7.46 (t, $J = 7.7$ Hz, 2H), 7.58 (t, $J =$ 7.4 Hz, 1H), 8.11 ppm (d, $J = 8.3$ Hz, 2H); ^{13}C NMR (500 MHz, $CDCl_3$): $\delta = 17.87$, 32.90, 44.86, 64.82, 128.40, 129.48, 129.92, 133.28, 166.11, 167.96, 176.05 ppm; MS: *m/z*: 270.3 $[M+Na]^+$; HRMS: *m/z* calcd for $C_{13}H_{13}NNaO_4$ $[M+Na]^+$: 270.0742; found: 270.0741.

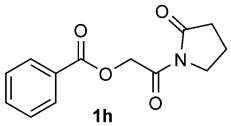

2-Oxo-2-(2-oxopyrrolidin-1-yl)ethyl 4-(dimethylamino)benzoate (1q): Compound **1q** was prepared according to the procedure in General Method A from **1v** and 4-(dimethylamino)benzoic acid on a 0.35 mmol scale. The crude product was purified by silica gel chromatography with a gradient of MeOH in CH_2Cl_2 (0 to 10%) to give **1q** (3.1 mg, 0.011 mmol). ^{1}H NMR (500 MHz, CDCl): $\delta = 2.09$–2.23 (m, 2H), 2.65 (t, $J = 8.1$ Hz, 2H), 3.07 (s, 6H), 3.87 (t, $J = 7.2$ Hz, 2H), 5.36 (s, 2H), 6.69 (d, $J = 9.0$ Hz, 2H), 8.00 ppm (d, $J = 9.0$ Hz, 2H); ^{13}C NMR (500 MHz, $CDCl_3$): $\delta = 17.90$, 32.99, 40.12, 44.88, 64.32, 110.69, 116.05, 131.74, 153.56, 166.39, 168.68, 175.99 ppm; MS: *m/z*: 291.1 $[M+H]^+$; HRMS: *m/z* calcd for $C_{15}H_{19}N_2O_4$ $[M+H]^+$: 291.1345; found: 291.1348.

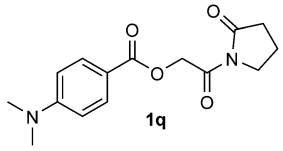

2-Oxo-2-(2-oxopyrrolidin-1-yl)ethyl 4-nitrobenzoate (1r): Compound **1r** was prepared according to the procedure in General Method A from **1v** and 4-nitrobenzoic acid on a 0.35 mmol scale.

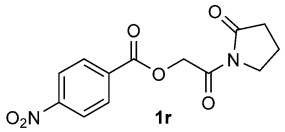

The crude product was purified by silica gel chromatography with a gradient of MeOH in CH_2Cl_2 (0 to 3%) to give **1r** (50.9 mg, 0.17 mmol). ^{1}H NMR (500 MHz, $CDCl_3$): $\delta = 2.02$–2.25 (m, 2H), 2.64 (t, $J = 8.1$ Hz, 2H), 3.84 (t, $J = 7.2$ Hz, 2H), 5.43 (s, 2H), 8.05–8.36 ppm (m, 4H); ^{13}C NMR (500 MHz, $CDCl_3$): $\delta = 17.91$, 32.85, 44.87, 65.40, 123.57, 131.06, 134.85, 150.72, 164.29, 167.34, 176.20 ppm; MS: *m/z*: 315.2 $[M+Na]^+$; HRMS: *m/z* calcd for $C_{13}H_{12}O_6N_2Na$ $[M+Na]^+$: 315.0588; found: 315.0594.

2-Oxo-2-(2-oxopyrrolidin-1-yl)ethyl quinoline-6-carboxylate (1ad): Compound **1ad** was prepared according to the procedure in General Method A from **1v** and quinolone-6-carboxylic acid on a

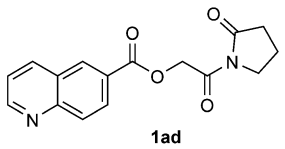

0.36 mmol scale. The crude product was purified by silica gel chromatography with a gradient of MeOH in CH_2Cl_2 (0 to 10%) to give **1ad** (26.6 mg, 0.089 mmol). ^{1}H NMR (500 MHz, $CDCl_3$): $\delta = 2.09$–2.32 (m, 2H), 2.66 (t, $J = 8.1$ Hz, 2H), 3.88 (t, $J = 7.2$ Hz, 2H), 5.49 (s, 2H), 7.42–7.63 (m, 1H), 8.18 (d, $J = 8.8$ Hz, 1H), 8.29 (d, $J = 7.6$ Hz, 1H), 8.38 (dd, $J = 8.8$, 1.8 Hz, 1H), 8.70 (d, $J = 1.4$ Hz, 1H), 8.97–9.16 ppm (m, 1H); ^{13}C NMR (500 MHz, $CDCl_3$): $\delta = 17.91$, 32.91, 44.88, 65.10, 121.87, 127.42, 127.50, 129.13, 129.90, 131.52, 137.38, 150.28, 152.63, 165.64, 167.85, 176.04 ppm; MS: *m/z*: 299.2 $[M+H]^+$; HRMS: *m/z* calcd for $C_{16}H_{14}N_2NaO_4$ $[M+Na]^+$: 321.0846; found: 321.0846.

2-Oxo-2-(2-oxopyrrolidin-1-yl)ethyl biphenyl-4-carboxylate (1ae): Compound **1ae** was prepared according to the procedure in General Method A from **1v** and biphenyl-4-carboxylic acid on a

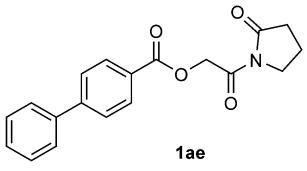

0.36 mmol scale. The crude product was purified by silica gel chromatography with a gradient of MeOH in CH_2Cl_2 (0 to 3%) to give **1ae** (49.2 mg, 0.15 mmol). ^{1}H NMR (500 MHz, $CDCl_3$): δ = 1.82–1.99 (m, 2H), 2.40 (t, J = 8.1 Hz, 2H), 3.62 (t, J = 7.2 Hz, 2H), 5.07 (s, 2H), 7.17 (t, J = 7.3 Hz, 1H), 7.25 (t, J = 7.5 Hz, 2H), 7.41 (d, J = 7.4 Hz, 2H), 7.46 (d, J = 8.3 Hz, 2H), 7.96 ppm (d, J = 8.3 Hz, 2H); ^{13}C NMR (500 MHz, $CDCl_3$): δ = 18.13, 33.17, 45.11, 65.10, 127.32, 127.54, 128.44, 129.18, 130.72, 140.18, 146.21, 166.23, 168.23, 176.33 ppm; MS: *m/z*: 346.3 $[M+Na]^+$; HRMS: *m/z* calcd for $C_{19}H_{17}NNaO_4$ $[M+Na]^+$: 346.1050; found: 346.1052.

Acknowledgements

Compounds for the HTS were provided by the National Screening Laboratory for the regional centers of excellence in biodefense and emerging infectious diseases (NIAID U54 AI057159). We thank Su Chaing and the staff at the NERCE National Screening Laboratory (NSRB) for assistance in performing the HTS and post-screen analysis, as well as Jonathan Venetz for comments on the manuscript. This research was supported by the ETH Zürich and by the National Institute of Allergy and Infectious Diseases (NIH, 1R21NS067579-01 and U54AI057141 to S.I.M, 1R21NS067579-01 to H.D.K, NSF Graduate Research Fellowship to B.R.K), the Swiss National Foundation (PA00P3-124140 and PBBSA-120489 to M.C. and PA00P3-126243 to B.C.), and the Novartis Foundation to M.C.

Conflict of Interest

The authors declare no conflict of interest.

Keywords: c-di-GMP · diguanylate cyclase inhibitors · FRET · high-throughput screening · structure–activity relationships

[1] L. R. Hoffman, D. A. D'Argenio, M. J. MacCoss, Z. Zhang, R. A. Jones, S. I. Miller, *Nature* **2005**, *436*, 1171 – 1175.
[2] E. Mills, I. S. Pultz, H. D. Kulasekara, S. I. Miller, *Cell. Microbiol.* **2011**, *13*, 1122 – 1129.
[3] D.-G. Ha, G. A. O'Toole, *Microbiol. Spectrum* **2015**, *3*, MB-0003 – 2014.
[4] M. J. Bush, N. Tschowri, S. Schlimpert, K. Flärdh, M. J. Buttner, *Nat. Rev. Microbiol.* **2015**, *13*, 749.
[5] S. Ozaki, A. Schalch-Moser, L. Zumthor, P. Manfredi, A. Ebbensgaard, T. Schirmer, U. Jenal, *Mol. Microbiol.* **2014**, *94*, 580 – 594.
[6] N. Ausmees, R. Mayer, H. Weinhouse, G. Volman, D. Amikam, M. Benziman, M. Lindberg, *FEMS Microbiol. Lett.* **2001**, *204*, 163 – 167.
[7] P. Aldridge, R. Paul, P. Goymer, P. Rainey, U. Jenal, *Mol. Microbiol.* **2003**, *47*, 1695 – 1708.
[8] C. Chan, R. Paul, D. Samoray, N. C. Amiot, B. Giese, U. Jenal, T. Schirmer, *Proc. Natl. Acad. Sci. USA* **2004**, *101*, 17084 – 17089.
[9] B. Christen, M. Christen, R. Paul, F. Schmid, M. Folcher, P. Jenoe, M. Meuwly, U. Jenal, *J. Biol. Chem.* **2006**, *281*, 32015 – 32024.
[10] M. Christen, H. D. Kulasekara, B. Christen, B. R. Kulasekara, L. R. Hoffman, S. I. Miller, *Science* **2010**, *328*, 1295 – 1297.
[11] B. R. Kulasekara, C. Kamischke, H. D. Kulasekara, M. Christen, P. A. Wiggins, S. I. Miller, *eLife* **2013**, *2*, e01402.
[12] E. Mills, E. Petersen, B. R. Kulasekara, S. I. Miller, *Sci. Signaling* **2015**, *8*, ra57.
[13] R. Paul, S. Weiser, N. C. Amiot, C. Chan, T. Schirmer, B. Giese, U. Jenal, *Genes Dev.* **2004**, *18*, 715 – 727.
[14] M. Folcher, S. Oesterle, K. Zwicky, T. Thekkottil, J. Heymoz, M. Hohmann, M. Christen, M. Daoud El-Baba, P. Buchmann, M. Fussenegger, *Nat. Commun.* **2014**, *5*, 5392.
[15] I. S. Pultz, M. Christen, H. D. Kulasekara, A. Kennard, B. Kulasekara, S. I. Miller, *Mol. Microbiol.* **2012**, *86*, 1424 – 1440.
[16] C. A. Kellenberger, S. C. Wilson, J. Sales-Lee, M. C. Hammond, *J. Am. Chem. Soc.* **2013**, *135*, 4906 – 4909.
[17] C. A. Kellenberger, J. Sales-Lee, Y. Pan, M. M. Gassaway, A. E. Herr, M. C. Hammond, *RNA Biol.* **2015**, *12*, 1189 – 1197.
[18] S. M. Ching, W. J. Tan, K. L. Chua, Y. Lam, *Bioorg. Med. Chem.* **2010**, *18*, 6657 – 6665.
[19] T. Kline, S. R. Jackson, W. Deng, C. L. M. J. Verlinde, S. I. Miller, *Nucleosides Nucleotides Nucleic Acids* **2008**, *27*, 1282 – 1300.
[20] D. L. Caly, D. Bellini, M. A. Walsh, J. M. Dow, R. P. Ryan, *Curr. Pharm. Des.* **2015**, *21*, 12 – 24.
[21] P. Ohana, D. P. Delmer, R. W. Carlson, J. Glushka, P. Azadi, T. Bacic, M. Benziman, *Plant Cell Physiol.* **1998**, *39*, 144 – 152.
[22] O. J. Lieberman, M. W. Orr, Y. Wang, V. T. Lee, *ACS Chem. Biol.* **2014**, *9*, 183 – 192.
[23] K. Sambanthamoorthy, R. E. Sloup, V. Parashar, J. M. Smith, E. E. Kim, M. F. Semmelhack, M. B. Neiditch, C. M. Waters, *Antimicrob. Agents Chemother.* **2012**, *56*, 5202 – 5211.
[24] K. Sambanthamoorthy, C. Luo, N. Pattabiraman, X. Feng, B. Koestler, C. M. Waters, T. J. Palys, *Biofouling* **2014**, *30*, 17 – 28.
[25] H. Weber, C. Pesavento, A. Possling, G. Tischendorf, R. Hengge, *Mol. Microbiol.* **2006**, *62*, 1014 – 1034.
[26] R. R. Spurbeck, R. J. Tarrien, H. L. T. Mobley, *mBio* **2012**, *3*, e00307-12-e00307-12.
[27] C. A. Lipinski, *J. Pharmacol. Toxicol. Methods* **2000**, *44*, 235 – 249.
[28] T. Ohashi, S. D. Galiacy, G. Briscoe, H. P. Erickson, *Protein Sci.* **2007**, *16*, 1429 – 1438.

Manuscript received: October 4, 2018
Accepted manuscript online: November 5, 2018
Version of record online: ■■ ■■, 0000

Controling biofilm formation: Diguanylate cyclases (DGCs) are attractive anti-invective drug targets for control of biofilm formation. We report a FRET-based HTS assay coupled with detailed structure–activity studies to identify modulators of DGCs. Detailed mechanism-of-action studies demonstrate the complex interplay between the synthetic compounds and the regulatory mechanisms that control the activity of DGCs.

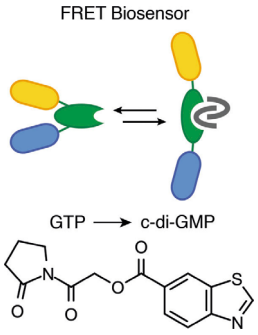

M. Christen, C. Kamischke, H. D. Kulasekara, K. C. Olivas, B. R. Kulasekara, B. Christen, T. Kline, S. I. Miller*

■■ – ■■

Identification of Small-Molecule Modulators of Diguanylate Cyclase by FRET-Based High-Throughput Screening